COARSE GRAINED MOLECULAR DYNAMIC SIMULATION OF BLOCK COPOLYMER DIRECTED SELF ASSEMBLY ON TOPOGRAPHIC SUBSTRATE

A Thesis

Presented to the Faculty of the Graduate School

of Cornell University

In Partial Fulfillment of the Requirements for the Degree of

Master of Science

by

Yufeng Qiu

August 2020

ABSTRACT

Directed self-assembly (DSA) of block copolymer (BCP) is a promising and economic method of manufacturing periodic lamellar patterns on wafer that is widely used in semi-conductor and electronic fields. In BCP DSA lithography, same as issues in achieving defective free patterns and smooth edges, an evenly distributed width line space pattern is also critical but in lack of research.

Comparing with experiment, simulation has many advantages on cost, accuracy and repeatability. Simulation has been very successful in predicting physical behaviors of systems and guiding the experiments.

In this research, a coarse grained molecular dynamic (CGMD) simulation on polystyrene-b-poly (methyl methacrylate) (PS-b-PMMA) block copolymer DSA process using chemoepitaxial method was carried out. By changing BCP composition, substrate properties including topography and interaction strength, their effects on produced lamellae critical dimension (CD) variation, line space variation, roughness and tapering effect were investigated. It gives the direction of optimizing the substrate structure.

BIOGRAPHICAL SKETCH

Yufeng Qiu was born in Qingdao, China on October 7th, 1996 and raised there. He has shown a love for chemistry since middle school. And after graduated form Qingdao No.2 High School in 2014, he went to East China University of Science and Technology which located in Shanghai, majored in Chemistry. Studying and solving chemistry every day was attractive and as the ranking first student, he won 2015 Chinese National Scholarship, but out of the desire of focusing more on the application side, he switched his major to Chemical Engineering in his sophomore year. After that, he took part in 2 parts of research in 2 years, one as a group research focusing on rheology of cellulose originated oil field fracturing fluid, the other as an individual research on polymer modified environment responsive silicon nanoparticle. At his senior year, Yufeng was sent to University of Houston by China Scholarship Council (CAC) to finish his senior design there. In 2018, after earning his Bachelor of Engineering degree from ECUST, he went to Cornell University to pursue Master of Science in Chemical Engineering under the supervision of Dr.Yong Lak Joo. He started with organic electrolyte flow battery program. Later in 2019, with the aim of exposing himself to more areas, he changed his focus area into modeling. Since then, he was working on the simulation of directed self assembly (DSA) of block copolymer (BCP) in order to control the defect and roughness of the generated line space structure. Working on this project helped him earned Graduate Research Assistantship (GRA) in 2019.

To mom, dad, all the other I love and loved

ACKNOWLEDGMENTS

I would like to express my most sincerely gratitude to my advisor Dr.Yong L. Joo, from the orientation day when he agreed to be my PI, he helped me so much in many perspectives in the past two years. He provided me many opportunities to work with industrial people, gave many useful advices whenever I felt lost in research. The more important thing is he showed me himself that what it takes to be outstanding, determined and diligent. I am so glad that I can still work with him in my PhD career. I am also grateful to Dr. Christopher Ober and Dr. Uli Wiesner, who serve as my committee members, their professionality also helped me a lot in understanding BCP DSA. The thanks also goes to Dr.Tobias Hanrath, Dr.Kathleen Vaeth and Dr. Brad Anton, they provided me TA opportunities in two semesters in which I learned a lot about product manufacturing and had the chance to communicate with so many excellent students.

I acknowledge and appreciate all the support and help from my friends here at Cornell. In particular I would like to thanks Dr.Shubham Pinge and Dr.George Shebert, their deep knowledge and ideas in simulation field really amazed and inspired me; Travis, Dr.Mounica Divvela, Chris, Chaowen, Naman, Ritika, Vaidik, and Cecilia, it was one of the most interesting and attractive things talking with them about random stuffs including religions and even existence; Emily for showing me another possibility of life; Nicole and Yiqi for sharing me so many laughs and stories, I am so glad I have friends like you two; and all the other Joo group members, you guys together made my two years full of enjoyable memories.

Finally, I would not be who I am today without the infinity love and support from my mom and dad, no words can express my gratitude to you. And Chang, not much to say, welcome to my life.

TABLE OF CONTENTS

LIST OF FIGURES

LIST OF TABLES

CHAPTER 1. INTRODUCTION

1.1 Block copolymer directed self-assembly overview

1.1.1 The need for using block copolymer directed self-assembly

While the demand for better performance and lower cost microelectronic devices is growing dramatically, the most promising candidate technologies for semiconductors under 7nm node, extreme ultraviolet (EUV) lithography method, has encountered many issues like unpredictable stochastic printing failures[1-3], relatively short pellicle membrane, mask and collector lifetime[4-6], scanner defectivity[4], the resist performance[7-9], etc. Over the past two decades, directed self-assembly (DSA) of block copolymers (BCPs) has attracted the interest of both academia and industry to develop optimal, defect free nanolithographic patterns and miniaturize semiconductors due to its low-cost. Also, it is not restricted by inherent diffraction-based limitation[10-14].

Due to the incompatibility between the components in BCP molecules, at equilibrium, BCP will self-organize at molecular level, build blocks and form nano-structures like hexagonally packed cylinders, lamellae, gyroids or spherical micelles with characteristic length scales to minimize the free energy. The obtained structure is determined by the type of monomers in BCP and the ratio of different type of monomers. For the micro-electronics industry, the lamellar structures are used as nano-templates in the manufacture of microchips, after etching off one type of monomers in lamellae structure, the remaining line-space patterns will have the same structure as what optimal lithography provides.

The multiplication property of BCP DSA is very useful in decreasing the demand for extremely high resolution requirement during lithography. It can be achieved even when the location of the guiding spots in the chemical pattern was randomly varied by as much as 23% of the natural domain spacing[15]. Although optical lithography is needed when generating the directing substrate, the demanded resolution will be many times smaller than that for EUV lithography. And the issues related with high energy generated in EUV process that could cause low lifetime can also be avoided by using BCP DSA method. With the improvement of defect and roughness control methods, this method can be a replacement for EUV in manufacturing devices like 7nm fin field effect transistor (FinFET)[16]. It is true that many areas are still remaining to be tackled to fully apply BCP DSA into industrial manufacturing, but its potential in producing microelectronic devices is really worth noticing and many people are dedicating themselves into this field.

1.1.2 The principle of BCP DSA

Normally, it is required for BCP to have a directed force to form demanded periodic spatial arrangement that can be used in industry[17]. The process of BCP DSA that is exclusively thermodynamically driven is slow, with limited control on the domain size and sometimes with poor degree of micro-phase separation. The morphology of the system may have a strong local order, but in many cases, in lack of long range orientation and translational order. A suitable directed force can not only control the obtained pattern orientation but also increase the structure formation speed.

DSA combined with advanced lithography techniques offers an additional driven force that provides orientational order to create patterns suitable for lithographic applications. Introduction of confinement effects in the form of external topography and surface features of the substrate called graphoepitaxy, or enthalpic effects like chemical patterning of the substrate and the features called chemoepitaxy can have a significant enhancement on the annealing time and the quality of the nano-pattern formed[18-24]. These are the two main methods that applied in industry to direct BCP self-assembly. Compared with chemoepitaxy, graphoepitaxy is harder to perform on a large scale to get lamellar structure, it is more often used to get ordered cylindrical domains or smaller scale lamellar structure.

Among chemoepitaxial technologies to form line space patterns, Liu-Nealey (LiNe) flow with near symmetric polystyrene-b-polymethyl methacrylate (PS-b-PMMA) has been widely considered as a prospective DSA candidate for commercialization[25-26]. This method starts with the deposition of a cross linking PS mat on silicon substrate, followed by lithographic patterning of a photoresist on top of the mat. Then the formed structure will be transferred to cross linking PS via an oxygen plasma etch. If the acquired width is higher than required, an optional “trim etch” will be carried out for fine dimension control, this is basically having more etching time after the normal etching (in the paper this was called “breakthrough etching”). After etching, the remaining photoresist will be removed using solvent. Different types of brushes are then grafted on the interspatial regions based on different functions[27]. To use a substrate which has different chemical preference towards BCP to direct its self-assembly, the substrates are normally composited of 2 parts, PS attractive regions and

neutral regions. Some of the systems have the third region, which can be preferable to PMMA or neutral, those systems are called "3-tone system"[28]. The PS-pinned region is patterned with cross-linked PS mat film while the rest of the substrate is grafted by random hydroxyl terminated PS-*b*-PMMA chains (neutral layer) usually of a lower chain length than the PS mat. Due to the etch when generating the pinned PS area, the unpinned area is polarized and attractive to PMMA if no brush is grafted on the top of it. As a result, at some area where brush graft density is low (for example on the inclined wall near PS pinned area), the substrate will acquire PMMA attractivity (3-tone system). PS-*b*-PMMA BCP is then spin coated on top of this chemically patterned substrate and annealed at elevated temperatures (250-300˚C) to obtain defect-free BCP lamellae.

After the BCP lamellae formation, the PMMA domain will be selectively etched off to form a line space pattern of PS. This PS pattern can be used in the following nano lithography process as a template. This etching process can be carried out with a selective solvent like acetic acid, this process is called wet etching. Or it can perform with a variety of plasma, named dry etching, in which O_2/Ar being the most popular etching gas[29-32]. Comparing with wet etching, dry etching is more commonly applied because there is no capillary forces during this process, so it will not lead to structure collapses. Some main issues in BCP DSA lithography including high roughness value (both line edge roughness (LER) and line width roughness (LWR)), defectiveness and critical dimension (CD) variation[33-36]. Those issues will hinder the usage of generated BCP line space pattern as the template for the microelectronic circuit production, as a result, they have to be studied to make this technic more practical and usable[37-38].

1.2 Simulation method overview

1.2.1 Types of simulation methods

Comparing with experiment, simulation has many advantages on cost, accuracy and repeatability. Theoretically, if we can take all the influential factors into consideration, the results will be the same as what is acquired in an ideal experiment. Although with current computing capacity, no matter on what simulation scale, many details will need to be ignored or the timescale will need to be extremely short. The good news is plenty of simulations have proven that there is no harm to neglect things either too small or too large than the simulation scale. Simulation has been very successful in predicting physical behaviors of systems and guiding the experiments. One thing needs to be mentioned is that simulation, especially simulation on substances (for example, BCP DSA), will be much more convincing and useful if it has been verified by corresponding experiment under similar conditions. Without a single experiment, sometimes it can be very tricky to prove the reliability of the model.

With the dramatic development of computational science both in software and hardware, simulation is therefore, becoming more powerful. The world ranking number 1 supercomputer Summit, an IBM built supercomputer now running at Department of Energy's (DOE) Oak Ridge National Laboratory (ORNL), can reach a speed 122.3 quadrillion floating-points operations per second (petaFLOPS). Even the world ranking 500 supercomputer Swiss National Supercomputing Center (CSCS) can

reach to a maximum speed of 0.72 petaFLOPS. Even though we are still unable to simulate a long time period starting from atom level, those blooming computing resources can ensure a better quality and reliability of simulation and bring the simulation to a longer time scale.

For some experiment, trying all the different conditions physically can be very costly and hard to manipulate. For instance, in BCP DSA, it is hard to only change the substrate raised level by few nanometers because there are many other parameters that will change together with varied etching conditions, like pinned area width. Therefore, it is not an easy task to investigate solely the raised level height influence on the formed BCP line space patterns. On top of that, precisely control the raised level height to be 3nm or 4nm is difficult. Under circumstances like these, simulation can be very useful. Think of that if there is a simulation model that can match well with a substrate system that has certain parameters, all we need to do later is to change the parameters we would like to investigate. In this way, every property's influence on BCP patterns can be studied as well as their combination effects without spending a lot time and money. Also, the results can be more accurate than experiment considering the unavoidable errors that will be introduced during experiments. Modeling can aid the manufacturer in this regard.

Based on the scale of the research area, different simulation methods are introduced. At atomic scale, density functional theory (DFT) is widely applied. This is a computational quantum mechanical modelling method used in physics, chemistry and materials science to investigate the electronic structure of many-body systems, in particular, atoms, molecules and the condensed phases. The many-electron system can

be determined by using functionals. This method allows the prediction and calculation of material behavior on the quantum mechanical consideration without knowing higher order parameters like fundamental material properties[39].

Ab initio molecular dynamic (MD) method is a method focused on a scale larger than DFT but smaller than MD. It usually simulates 10^2 to 10^4 atoms. This method applies Newton's second law together with DFT to the atomic coordinates, the nuclei is regarded fixed at the instantaneous positions of the atoms using Born-Oppenheimer approximation. As a result, a time-dependent Schrödinger equation for the electrons wavefunction can be obtained. This equation is then be solved using DFT to obtain the energy, and this energy is considered to be a function of the previously fixed nuclear coordinate. Thus, this energy can be used as a field to calculate nuclei's motion using Newton's equation. By computing the DFT energy at a fixed point with corresponding to nuclear coordinate, the forces can be obtained and the next fixed point position can be calculated accordingly. Then the DFT calculation will be carried out again. Comparing with traditional MD method, this method can be used in the systems where parameters like bonding, polarization have not been determined[40].

Classic MD method is a method using Newton's second law to predict the position of every particles in each timestep. Parameters like bond type and energy are given. Normally, atom is regarded as an undivided structure, there is no need to solve the wavefunction for the electrons. Obviously, by ignoring electrons and nuclei, the scope of this method is larger than the ab initio MD. This method can be applied to 10^7 atoms level. This scope is enough to investigate molecules motion, but only in few nano seconds. The simulation scale can be increased by applying coarse-grained MD

(CGMD), which is regarding many atoms as a whole and ignore some properties like bond energy. The coarse-grained level is decided according to the system size. It can be a tricky thing to find a proper coarse-grain, but once found, this method is really useful in simulating molecules.

If the desired simulation scale keeps growing, continuum simulation will be used. By neglecting all the small particles but focusing them as a whole object, things like fluids or chemical reactions can be simulated using this type of method.

Monte-Carlo simulation is also a widely accepted simulating method in many fields, from social science to engineering, and can even be applied to the law and design fields. Different from MD, it imposes arbitrary moves on particles, and based on the energy state after the moving, a percentage of accepting this move is calculated and this percentage is applied to decide whether the original arbitrary move will happen. Due to its principle, this method can be used in solving any problems that have a probabilistic interpretation, not only in chemical field, it can also be used in solving economic problem like business risk management and math problem like evaluation of multidimensional definite integrals with complicated boundary conditions[41]. The scale of Monte Carlo method is therefore hard to define, it is able to be used from atom level all the way to continuum level, and it can be extended to the area wider than that.

1.2.2 Basic of CGMD method

Many simulation works have been done towards BCP DSA include using Self-Consistent Field (SCF), Theoretically Informed Coarse-Grained (TICG) framework,

and MD[42-45]. SCF method can predict the BCP phase diagrams but has problem measuring the fluctuations, as a result, interfacial width. TICG is better at calculating fluctuation and therefore provides a good method in studying BCP DSA, it performs very well in forecasting the energies of defect annihilation[46-47]. Dauloas and co-authors have studied the effect of roughness of the patterned substrate and its propagation through the film thickness, for undulated and peristaltic low frequency variation using a SCMF approach with successful comparison with experiments[48-49]. Segal-Peretz and co-workers have demonstrated the implementation of TICG in conjunction with scanning transmission electron microscopy (STEM) to characterize the three-dimensional structure of DSA with high-χ BCP, P2VP-*b*-PS-*b*-P2VP[50]. However, due to the high degree of coarse-graining, the roughness values obtained from TICG or related method as Single-Chain-in-Mean-Field (SCMF) are only able to represent the roughness in low-frequency region precisely, the high-frequency area is hard to represent. Among the MD literature on the subject, there is a lack of matching of the BCP chain length to the actual molecular weight and the corresponding experimental BCP pitch (L_0).

These simulations are computationally economical, however, none of the above stated works have studied the resist morphology evaluation after etching one of the BCP phases, which is of crucial importance. Our group has created a CGMD model that can represent both low and high frequency BCP area, and this model can be used to simulate all the process including etching in the BCP DSA. This simulation model has been verified using experimental data.

Reference

(1). P.De Bisschop, E. Hendrickx. Stochastic effect in EUV lithography. Proc. SPIE, 105831K (2018).

(2). C. Mack. Line-edge roughness and the ultimate limit of lithography. Proc. SPIE, 763931 (2010).

(3). P.De Bisschop. Impact of stochastic effect on EUV printability limit. Proc. SPIE, 904809 (2014).

(4). Seong-Sue Kim, et al. Progress in EUV lithography toward manufacturing. Proc. SPIE, 10143 (2017).

(5). Seong-Sue Kim, et al. EUV mask imaging system based on the scanning reflective microscopy. EUVL Symposium, Toyama (2013).

(6). Derk Brouns, et al. NXE Pellicle: offering a EUV pellicle solution to the industry. Proc. SPIE, 97761Y-1 (2016).

(7). Tatsuya Fujii, Shogo Matsumaru, Tomotaka Yamada, Yoshitaka Komuro, Daisuke Kawana, Katsumi Ohmori. Patterning performance of chemically amplified resist in EUV lithography. Proc. SPIE, 97760Y (2016).

(8). Yoshitaka Komuro, et al. Acid generation mechanism in anion-bound chemically amplified resists used for extreme ultraviolet lithography. Proc. SPIE, 9422O (2015).

(9). Takahiro Kozawa, et al. Acid generation efficiency in a model system of chemically amplified extreme ultraviolet resist. Journal of Vacuum Science Technology B, Vol. 24, No.6, L27 (2006).

(10). Jeong SJ, Kim JY, Kim BH, Moon HS, Kim SO. Directed self-assembly of block copolymers for next generation nanolithography. Materials Today. 2013 Dec 31;16(12):468-76.

(11). Liu CC, Ramírez-Hernández A, Han E, Craig GS, Tada Y, Yoshida H, Kang H, Ji S, Gopalan P, de Pablo JJ, Nealey PF. Chemical patterns for directed self-assembly of lamellae-forming block copolymers with density multiplication of features. Macromolecules. 2013 Feb 11;46(4):1415-24.

(12). Ruiz R, Kang H, Detcheverry FA, Dobisz E, Kercher DS, Albrecht TR, de Pablo JJ, Nealey PF. Density multiplication and improved lithography by directed block copolymer assembly. Science. 2008 Aug 15;321(5891):936-9.

(13). Mack CA. Field guide to optical lithography. Bellingham, Washington, USA: SPIE Press; 2006 Jan 24.

(14). Wu B, Kumar A. Extreme ultraviolet lithography: a review. Journal of Vacuum Science & Technology B. 2007 Nov 1;25(6):1743-61.

(15). Chi Chun Liu, et al. Chemical patterns for directed self-assembly of lamellae-forming block copolymers with density multiplication of features. Macromolecules, 2013, 46: 1415-1424.

(16). Kafai Lai, et al. Design technology co-optimization assessment for directed self-assembly-based lithography: design for directed self-assembly or directed self-assembly for design? Proc. SPIE, 013502 (2017).

(17). Bates FS, Fredrickson GH. Block copolymers-designer soft materials. Physics today. 2000.
(18). Segalman RA, Schaefer KE, Fredrickson GH, Kramer EJ, Magonov S. Topographic templating of islands and holes in highly asymmetric block copolymer films. Macromolecules. 2003 Jun 17;36(12):4498-506.
(19). KG AT, Gotrik KW, Hannon AF, Alexander-Katz A, Ross CA, Berggren KK. Templating three-dimensional self-assembled structures in bilayer block copolymer films. Science. 2012 Jun 8;336(6086):1294-8.
(20). Pinge S, Lin G, Padmanaban M, Baskaran D, Joo YL. Designing an Ordered Template of Cylindrical Arrays based on a Simple Flat Plate Confinement of Block Copolymers: A Coarse-Grained Molecular Dynamics Study. Soft Matter. 2017. DOI: 10.1039/C7SM02015E.
(21). Cheng JY, Rettner CT, Sanders DP, Kim HC, Hinsberg WD. Dense self-assembly on sparse chemical patterns: Rectifying and multiplying lithographic patterns using block copolymers. Advanced Materials. 2008 Aug 18;20(16):3155-8.
(22). Kim SO, Solak HH, Stoykovich MP, Ferrier NJ, de Pablo JJ, Nealey PF. Epitaxial self-assembly of block copolymers on lithographically defined nanopatterned substrates. Nature. 2003 Jul 24;424(6947):411-4.
(23). Liu CC, Han E, Onses MS, Thode CJ, Ji S, Gopalan P, Nealey PF. Fabrication of lithographically defined chemically patterned polymer brushes and mats. Macromolecules. 2011 Mar 18;44(7):1876-85.
(24). Liu CC, Ramírez-Hernández A, Han E, Craig GS, Tada Y, Yoshida H, Kang H, Ji S, Gopalan P, de Pablo JJ, Nealey PF. Chemical patterns for directed self-assembly of lamellae-forming block copolymers with density multiplication of features. Macromolecules. 2013 Feb 11;46(4):1415-24.
(25). Liu CC, Nealey PF, Ting YH, Wendt AE. Pattern transfer using poly (styrene-block-methyl methacrylate) copolymer films and reactive ion etching. Journal of Vacuum Science & Technology B: Microelectronics and Nanometer Structures Processing, Measurement, and Phenomena. 2007 Nov;25(6):1963-8.
(26). Muramatsu M, Iwashita M, Kitano T, Toshima T, Somervell M, Seino Y, Kawamura D, Kanno M, Kobayashi K, Azuma T. Nanopatterning of diblock copolymer directed self-assembly lithography with wet development. Journal of Micro/Nanolithography, MEMS, and MOEMS. 2012 Jul 1;11(3):031305-1.
(27). Chi Chun Liu, et al. Fabrication of lithographically defined chemically patterned polymer brushes and mats. Macromolecules, 2011, 44: 1876-1885.
(28). Lance D. Williamson, et al. Three-tone chemical patterns for block copolymer directed self-assembly. Applied materials and interfaces, 2016, 8, 4: 2704-2712.
(29). Black CT, Guarini KW, Milkove KR, Baker SM, Russell TP, Tuominen MT. Integration of self-assembled diblock copolymers for semiconductor capacitor fabrication. Applied Physics Letters. 2001 Jul 16;79(3):409-11.
(30). Gharbi A, Tiron R, Pimenta Barros P, Argoud M, Servin I, Chevalier X, Nicolet C, Navarro C. PMMA removal options by wet development in PS-b-PMMA block copolymer for nanolithographic mask fabrication. Journal of

Vacuum Science & Technology B, Nanotechnology and Microelectronics: Materials, Processing, Measurement, and Phenomena. 2015 Sep;33(5):051602.
(31). Chung TY, Nest D, Graves DB, Weilnboeck F, Bruce RL, Oehrlein GS, Wang D, Li M, Hudson EA. Electron, ion and vacuum ultraviolet photon effects in 193 nm photoresist surface roughening. Journal of physics D: Applied physics. 2010 Jun 21;43(27):272001.
(32). Nest D, Chung TY, Vegh JJ, Graves DB, Bruce RL, Lin T, Phaneuf RJ, Oehrlein GS, Long BK, Willson CG. Role of polymer structure and ceiling temperature in polymer roughening and degradation during plasma processing: a beam system study of P4MS and PαMS. Journal of Physics D: Applied Physics. 2010 Feb 12;43(8):085204.
(33). Ting YH, Liu CC, Park SM, Jiang H, Nealey PF, Wendt AE. Surface roughening of polystyrene and poly (methyl methacrylate) in Ar/O2 plasma etching. Polymers. 2010 Dec 2;2(4):649-63.
(34). Zekonyte J, Zaporojtchenko V, Faupel F. Investigation of the drastic change in the sputter rate of polymers at low ion fluence. Nuclear Instruments and Methods in Physics Research Section B: Beam Interactions with Materials and Atoms. 2005 Jul 1;236(1-4):241-8.
(35). Gronheid R, Delgadillo PR, Pathangi H, Heuvel D, Parnell D, Chan BT, Lee Y, Look LV, Cao Y, Her Y, Lin G, Harukawa R, Nagaswami V, D'Urzo L, Somervell M, Nealey P. Defect reduction and defect stability in IMEC's 14nm half-pitch chemo-epitaxy DSA flow. SPIE Advanced Lithography, 2014, 9049: 904905.
(36). Delgadillo PR, Suri M, Durant S, Cross AJ, Nagaswami VR, Heuvel D, Gronheid R, Nealey P. Defect source analysis of directed self-assembly process. Journal of Micro/Nanolithography, MEMS, and MOEMS, 2013, 12(3): 031112.
(37). Baravelli E, Dixit A, Rooyackers R, Jurczak M, Speciale N, De Meyer K. Impact of line-edge roughness on FinFET matching performance. IEEE Transactions on Electron Devices. 2007 Sep;54(9):2466-74.
(38). Leung G, Lai L, Gupta P, Chui CO. Device-and circuit-level variability caused by line edge roughness for sub-32-nm FinFET technologies. IEEE Transactions on Electron Devices. 2012 Aug;59(8):2057-63.
(39). Dorian A. H. Hanaor, Mohammed H. N. Assadi, Sean Li, Aibing Yu, Charles C. Sorrell. Ab initio study of phase stability in doped TiO_2. Computational Mechanics, 2012, 50: 185-194.
(40). Dominik Marx, Jurg Hutter. Ab initio molecular dynamics: theory and implementation. Modern methods and algorithm of quantum chemistry. 2000: 301-449.
(41). Douglas Hubbard, Douglas A. Samuelson. Modeling without measurements. OR/MS Today, 2009 (10): 28-33.
(42). Matsen MW, Bates FS. Unifying weak-and strong-segregation block copolymer theories. Macromolecules. 1996 Feb 12;29(4):1091-8.

(43). Detcheverry FA, Pike DQ, Nagpal U, Nealey PF, de Pablo JJ. Theoretically informed coarse grain simulations of block copolymer melts: method and applications. Soft Matter. 2009;5(24):4858-65.
(44). Peters AJ, Lawson RA, Ludovice PJ, Henderson CL. Detailed molecular dynamics studies of block copolymer directed self-assembly: Effect of guiding layer properties. Journal of Vacuum Science & Technology B, Nanotechnology and Microelectronics: Materials, Processing, Measurement, and Phenomena. 2013 Nov;31(6):06F302.
(45). Peters AJ, Lawson RA, Ludovice PJ, Henderson CL. Effects of block copolymer polydispersity and χN on pattern line edge roughness and line width roughness from directed self-assembly of diblock copolymers. InProc SPIE 2013 Mar 26 (Vol. 8680, pp. 868020-1).
(46). Hur SM, Thapar V, Ramírez-Hernández A, Khaira G, Segal-Peretz T, Rincon-Delgadillo PA, Li W, Müller M, Nealey PF, de Pablo JJ. Molecular pathways for defect annihilation in directed self-assembly. Proceedings of the National Academy of Sciences. 2015 Nov 17;112(46):14144-9.
(47). Hur SM, Khaira GS, Ramírez-Hernández A, Müller M, Nealey PF, de Pablo JJ. Simulation of defect reduction in block copolymer thin films by solvent annealing. ACS Macro Letters. 2014 Dec 11;4(1):11-5.
(48). Daoulas KC, Müller M, Stoykovich MP, Kang H, de Pablo JJ, Nealey PF. Directed copolymer assembly on chemical substrate patterns: A phenomenological and single-chain-in-mean-field simulations study of the influence of roughness in the substrate pattern. Langmuir. 2008 Feb 19;24(4):1284-95.
(49). Stoykovich MP, Daoulas KC, Müller M, Kang H, de Pablo JJ, Nealey PF. Remediation of line edge roughness in chemical nanopatterns by the directed assembly of overlying block copolymer films. Macromolecules. 2010 Feb 10;43(5):2334-42.
(50). Segal-Peretz T, Ren J, Xiong S, Khaira G, Bowen A, Ocola LE, Divan R, Doxastakis M, Ferrier NJ, de Pablo J, Nealey PF. Quantitative three-dimensional characterization of block copolymer directed self-assembly on combined chemical and topographical prepatterned templates. ACS nano. 2017 Jan 17;11(2):1307-1319.

Chapter 2. ANALYZING METHODS FOR BCP STRUCTURE

2.1 Introduction

The two main constraint factors for BCP DSA is roughness and defectiveness, besides those, other properties like critical dimension (CD) variation and line-space variation are also important in determining a lamellar structure's performance. CD variation is the difference between the width of PS domains that on top of the pinned area and the width of PS domains on top of the unpinned area. Line-space variation is the difference between PS domains and PMMA domains. In microelectronic device manufacturing field, both Metal Oxide Semiconductor Field Effect Transistor (MOSFET) and fin Field Effect Transistor (FinFET) are required lamellae structure to begin with, and that is the process where BCP DSA can be used[1]. For those lamellae structure, the goal is always to have the lowest possible roughness values (line edge roughness (LER) and line width roughness (LWR)), the lowest CD variation and the lowest line-space variation as well. Because after BCP lamellae formation, one type of monomer will be etched off, the remaining structure should have exact line width to ensure better performance of the microelectronic devices generated from that. The distance between those lines (space variation) should also be the same, and this distance is required to be close to the line width.

The basic of understanding everything happened in the system is to have a set of useful analyzing tools that can represent the system properties accurately and efficiently. In industry, what people mostly rely on is scanning electron microscope (SEM), transmission electron microscope (TEM) and scanning transmission electron

microscope (STEM)[2-5]. Ting-Ya Lo, et al used 3D TEM to investigate the order-order transition (OOT) in polystyrene block polydimethylsiloxane (PS-b-PDMS) BCP in order to address the problem which usually shows up in 2D TEM, it is difficult to elucidate the details of the 3D grains nucleated in the OOT process from 2D projection[6]. Kevin Gotrik et al used SEM and 3D TEM methods on PS-b-PDMS BCP, they compared the experimental results with the simulation results came from SCFT at before and after etching stages[7]. Segal Peretz et al combined sequential infiltration synthesis (SIS) and STEM in PS-b-PMMA system with the aim of enhancing image contrast to obtain better image quality and therefore analyze the lamellar structure more accurately[1],[8-13]. Those methods are very helpful but have their own disadvantages such as resolution, unable to detect detailed 3D structure inside each domain, etc. While those disadvantages are unavoidable in industrial production, in simulation, there are many ways to analyze the lamellar structure through out the whole domains accurately and efficiently. Because all particles coordinates can be known, to analyze the structure, what left is to find the suitable methods and optimize them.

2.2 3D Roughness Analyzing Method

Figure 2.1 is an illustration graph for BCP lamellae in simulation. In this trial, the averaged molecular weight for PS and PMMA are both 26,000 g/mol, averaged chain length for PS in one BCP molecular is 63, for PMMA is 58, poly distribution index (PDI) = 1.01. Total simulation box dimension is x*y*z = 90*90*30, for substrate, the

substrate thickness is 3 nm, the gap between raised level (yellow) and bottom level (blue) is 4 nm, the pinned area width is 15 nm, the inclined wall distance is 30 nm. Red beads are PS, orange beads are PMMA, blue beads are bottom layer substrate, white beads are inclined wall, yellow beads are pinned area.

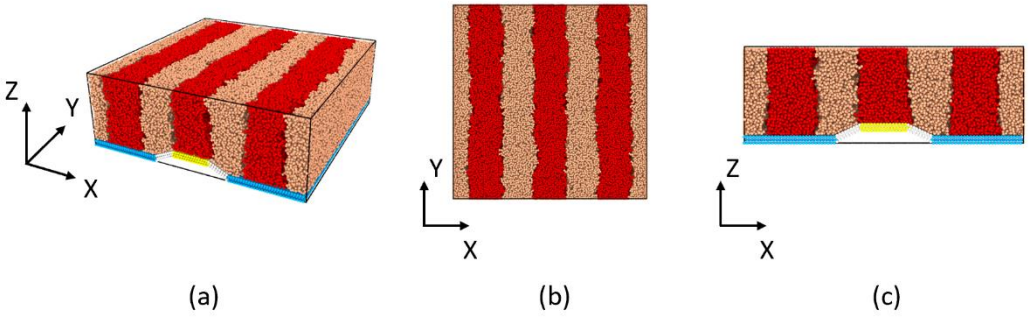

Figure 2.1. Simulated BCP lamellar structure after cooling viewing from 3 perspectives.

To clearly observe the roughness difference in different layers and its changing process during BCP annealing, it is vitally important to be able to calculate the roughness not only on the top layer (as what people are able to do using SEM images) but also through out the whole domain. In simulation, this is not a hard task. Because every beads' coordinates can be known, the simulation box can be "sliced" into many layers on z axis, and each layer's roughness will be calculated. Also, every certain timestep's coordinate (based on the need of us) data will be stored. In this way, both BCP structure changes with annealing time and position can be known. By finding the coordinates of each domain's edge beads, their width and roughness can be calculated. In my simulation, every layer is 1.3 nm in thickness and each layer's distance with

others is 2 nm, the coordinate data were stored every 0.2 million timesteps with a timestep equals to 0.01τ (a simulation unit for time in Lennard-Jones unit).

The results for the same trial as in figure 2.1 are shown in figure 2.2. The properties that were used to measure roughness here are line width roughness (LWR), which is the standard deviation of widths at every part of PS domains and line edge roughness (LER), which is the standard deviation of the edge beads deviate from the average edge lines. To accommodate with industrial standard, use 3σ values here, which is 3 times the standard deviation values.

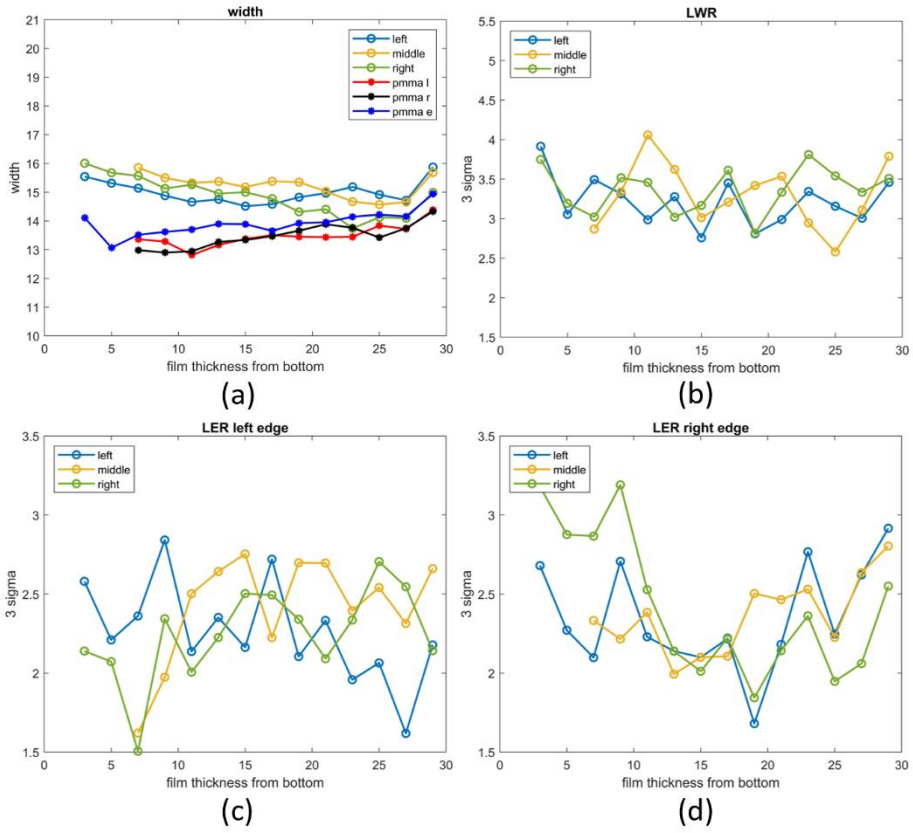

Figure2.2. a) all 6 domain widths, b) PS domains LWR, c) PS domains LER on the left edges and d) PS domains LER on the right edges on different z axis results after

cooling, each point is the average value of 15 time steps after lamellar structure has formed in order to eliminate the fluctuation.

2.3 3D Defective Analyzing Method

Defectiveness is a crucial property for the judgement for the quality of BCP structures. There are many kinds of defective, micro-bridge, dislocation, etc[14-18]. In industrial, people are using automatic software to distinguish the amount and type of defectiveness in a relatively large area (~cm^2). In simulation, due to the small area of the simulation box (~knm^2) and higher analyzable data quality, there is no need to use the industrial tools. On top of that, defective type difference is not the focus point of the current research, knowing the quality of BCP structure is sufficient. Therefore, an algorithm that can divide defective into 2 types (continuous defect and discontinuous defect) automatically is created as shown in figure 2.3. The original beads coordinates will be converted into a bicolor image to find the edge of PS and PMMA. Gaussian filter is used and every 10 pixels are averaged into one value to blur the edge. In this way, the smooth edge lines can be obtained as in figure 2.3b. Then, by analyzing the angles at every corner, those defects can be found and divided into discontinuous and continuous defect as in figure 2.3c.

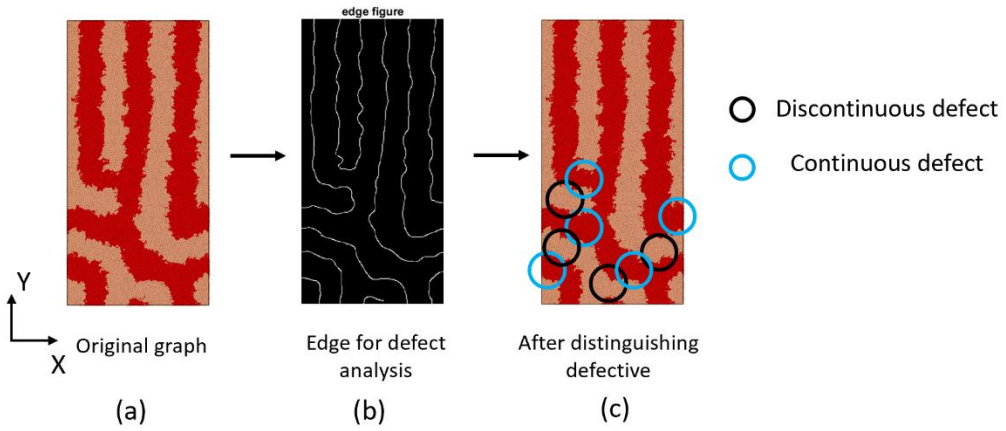

Figure 2.3. Automatic algorithm that can calculate defective amount in a BCP structure and divides them into discontinuous defect and continuous defect. a) original graph, b) bicolor graph with smooth edge lines, c) graph with defect amount and type.

Besides this automatic algorithm, a factor called “departure factor” (DF) is created to represent the amount of defect quantitatively. After the settlement of BCP chain length, BCP monomer ratio and substrate structure, the desired lamellae position is fixed. Any beads that appear at the undesired position can be regarded as defect. Therefore, after the annealing process, the amount of PS beads that are not at desired position over total amount of PS beads can be used to represent the amount defectiveness. But even under total random condition, this ratio cannot reach 1, based on different substrate and BCP composition, this value will be a little bit smaller than 0.5. To make DF more intuitive, the ratio is linear stretched to a range between 0 and 1. 0 means defect free lamellae while 1 means totally random distribution. After this stretching, sometimes DF can be larger than 1, especially at before annealing stage. Figure 2.4 shows an annealing process analyzing using DF. Even though after

annealing, DF is still larger than 0, this structure can be considered as a defect free lamellae. From figure 2.4b), the conclusion can be made that quantitatively, DF is sufficient to represent the BCP structure defect. Combined with defect distinguish algorithm, the defect analyze in simulation can be carried out.

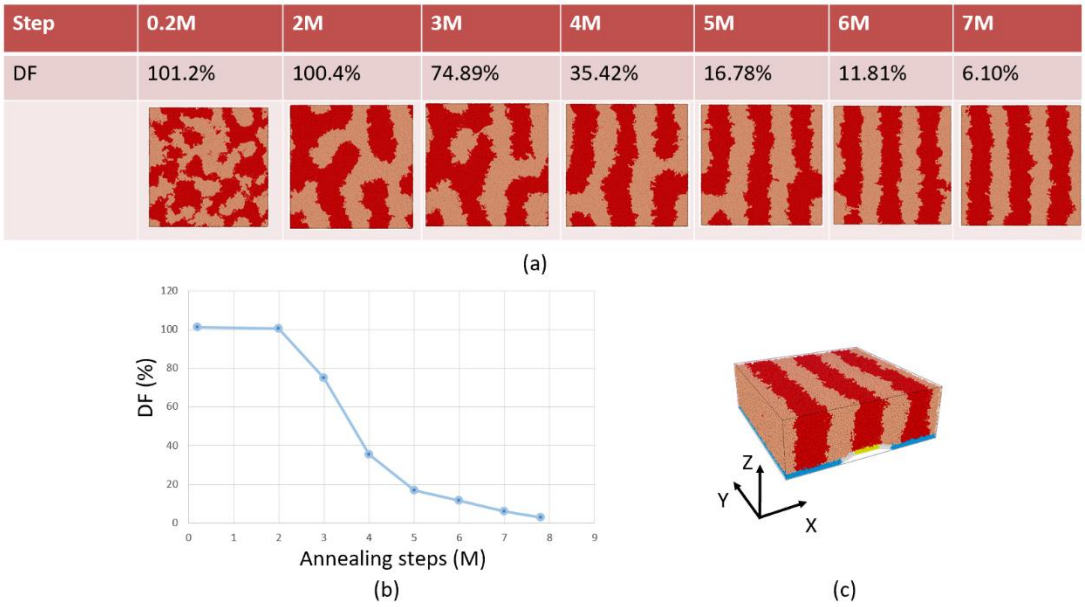

Figure 2.4. a) top view of the BCP structure during annealing stage and DF under each timestep, b) DF changes with annealing steps, c) the BCP lamellae structure after annealing

2.4 Width calculation method

In case of width calculation, if using the 3D edge detection method shows in section 2.2, it is also required to calculate the average value among each frame. That is because even after the BCP lamellae structure formation, the beads are still moving around and causing the boundaries fluctuating. As a result, in each frame, the width

will be different. However, according to our research, after the lamellae structure formation, every bead will stay within its original domain. In another word, the population of beads in each domain is fixed as shown in figure 2.5a. The density colormaps observed from 2 directions of both BCP monomers and total BCP beads are shown in figure 2.5b. To get the colormap, the simulation box was divided into many small 1 nm * 1 nm * 1 nm boxes, and the bead population is counted in each small box, different colors were given based on the population. The color more inclined to blue, the less beads there are, red vice versa. The smaller box size can be varied, considering the total simulation box size is 90 nm * 90 nm * 30 nm, the 1 nm^3 unit is suitable for density calculation. From these figures, it is obvious that the beads density is evenly distributed in the whole domain, while at the edge of each domain there is a very thin layer of "beads disappearing layer". Due to this property, a width calculation method called "back calculation" can be created. Since the beads' population and density in each domain can be obtained, and the total height on Z direction is fixed by the simulation box, the width of each domain can be calculated using equation 2.1. Via this method, the width fluctuation issue can be solved. Note that figure 2.5 is the same BCP trial as in figure 2.1 and 2.2.

$$width = \frac{domain\ population}{domain\ beads\ density} \frac{1}{Y*Z} \qquad \text{(equation 2.1)}$$

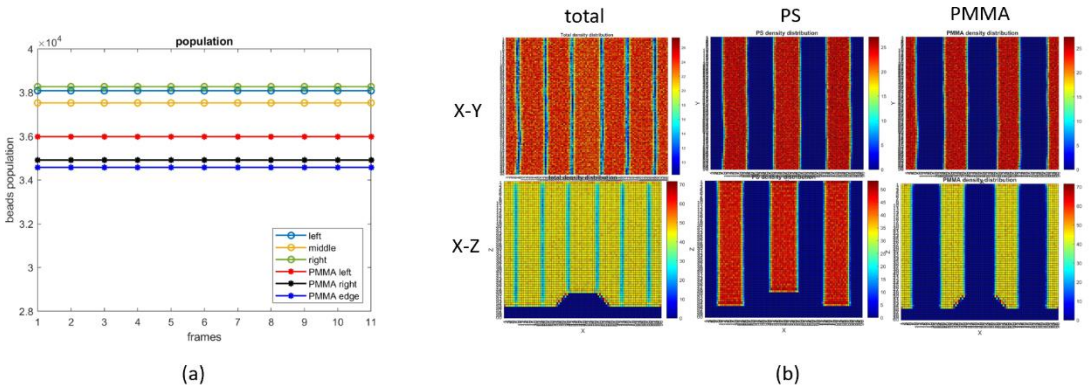

Figure 2.5. a) population changing with frames, b) density colormaps, the first row is looking from X-Y direction, the second row is looking from X-Z direction, the first column is total beads density, the second column is PS beads only and the third column is PMMA beads only.

2.5 Conclusion

Combining edge detection method with automatic defect algorithm and departure factor, the defectiveness of BCP lamellar structure can be measured and analyzed. Edge detection method and back calculation method are two ways of calculating line width in order to obtain CD variation and line-space variation. With these methods, the simulated BCP structure can be analyzed clearly and accurately.

Since these methods are the prerequisites of BCP simulation, and the simulation model we used has already been verified[19], we can then investigate varied parameters' influence on BCP line space patterns and from that, optimize those factors that influence BCP formation and give some suggestions to guide industrial manufacturing.

REFERENCES

(1). Hsinyu Tsai, et al. High chi block copolymer DSA to improve pattern quality for FinFET device fabrication. Proceedings of SPIE, 2016, 9779: 977910.

(2). Chun-Ku Chen, et al. Single helix to double gyroid in chiral block copolymers. Macromolecules. 2010, 43: 8637-8644.

(3). Kazuhiro Yamauchi, et al. Microdomain morphology in an ABC 3-miktoarm star terpolymer: a study by energy-filtering TEM and 3D electron tomography. Macromolecules, 2003, 36: 6962-6966.

(4). Jueun Jung, et al. Effect of film thickness on the phase behaviors of deblock copolymer thin film. ACS Nano, 2010, 4(6): 3109-3116.

(5). Vincent H. Mareau, et al. Direct visualization of the perforated layer/gyroid grain boundary in a polystyrene-block-polyisoprene/polystyrene blend by electron tomography. Macromolecules, 2007, 40: 9032-9039.

(6). Ting-Ya Lo, et al. Direct visualization of order-order transitions in silicon-containing block copolymers by electron tomography. ACS Macro Letters, 2013, 2(3): 190-194.

(7). Kevin W. Gotrik, et al. 3D TEM tomography of templated bilayer films of block copolymers. Advanced Functional Materials, 2014, 24: 7689-7697.

(8). Tamar Segal-Peretz, et al. Metrology of DSA process using TEM tomography. Proceedings of SPIE, 2015, 9424: 94240U-1.

(9). Hsinyu Tsai, et al. Teo-dimensional pattern formation using graphoepitaxy of PS-b-PMMA block copolymers for advanced FinFET device and circuit fabrication. ACS Nano, 2014, 8(5): 5227-5232.

(10). Chi-Chun Liu, et al. DSA patterning options for FinFET formation at 7nm node. Proceedings of SPIE, 2016, 9777: 97770R.

(11). Chi-Chun Liu, et al. Fin formation using graphoepitaxy DSA for FinFET device fabrication. Proceedings of SPIE, 2015, 9423: 94230S.

(12). Kafai Lai, et al. Design technology co-optimization assessment for directed self-assembly-based lithography: design for directed self-assembly or directed self-assembly for design? Journal of Micro/Nanolithography, MEMS, and MOEMS, 2017, 16(1): 013502.

(13). Hsinyu Tsai, et al. Electrical characterization of FinFETs with fins formed by directed self assembly at 29 nm fin pitch using a self-aligned fin customization scheme. IEEE International Electron Devices Meeting, 2014.

(14). Roel Gronheid, et al. Process optimization of templated DSA flows. Proceedings of SPIE, 2014, 9051: 905101.

(15). C. Simao, et al. Defect analysis and alignment quantification of line arrays prepared by directed self-assembly of a block copolymer. Proceedings of SPIE, 2014, 9050: 905028.

(16). Takeshi Kato, et al. Advanced CD-SEM metrology for pattern roughness and local placement of lamellar DSA. Proceedings of SPIE, 2014, 9050: 90501T.

(17). Lance Williamson, et al. Impact of BCP asymmetry on DSA patterning performance. Proceedings of SPIE, 2015, 9423: 942315.

(18). Chun Zhou, et al. Studying the effects of chemistry and geometry on DSA hole-shrink process in three-dimensions. Journal of Micro/Nanolithography, MEMS, and MOEMS, 2018, 17(3): 031203.
(19). Shubham Pinge, et al. Three dimensional line edge roughness in pre- and post-dry etch line and space patterns of block copolymer lithography. Physical Chemistry Chemical Physics, 2020, 22: 478-488.

CHAPTER 3. Computational Simulation of Different Topography Substrates Effects on CD and Line-Space Variation in Block Copolymer Directed Self-assembly

3.1 Introduction

Over the past decade, with the ever-increasing demand for miniaturization of micro- electronic devices, DSA of BCP has attracted the interest of both academia and industry to develop optimal, defect free nanolithographic patterns due to its low cost and it is not restricted by inherent diffraction-based limitation[1-4]. In particular, DSA technology using chemoeiptaxial Liu-Nealey (LiNe) flow to form line space patterns has been widely considered as a prospective candidate for commercialization and the replacement for expensive Extreme-Ultraviolet (EUV) lithography that can be used in manufacture of 7nm nodes and below [5-11].

BCP molecules can self-organized at molecular level, building blocks and periodic pattern structures like lamellae, hexagonally packed cylinders, gyroids and spherical micelles based on the fraction of each type of monomers in BCP. The system this research focused on is PS-b-PMMA block copolymer, in which the weight percentage of PS and PMMA are varying but kept close to 50% each (the most deviation is PS 43 wt.%, PMMA 57 wt.%). This fraction would give out a lamellar structure. The self-assembly process without any guidance normally takes a long time and the obtained shape is randomly oriented. With a suitable direct, this self-organized process will acquire a better kinetics performance and the direction it formed can be controlled.

Chemoepitaxy is an effective method which uses chemical affinity difference to guide the BCP self-assembly. LiNe flow is the method applied in this research to generate a substrate that can be used in chemoepitaxial method, an ideal topography is a flat substrate[12]. But it is not easy to generate a flat structure, some topographic structures will come out during the process of producing substrate[13]. For example, when forming the substrate to direct PS-b-PMMA self-assembly, the cross-linked PS will form a plateau structure with inclined edges higher than the adjacent neutral PS PMMA brushes. However, research shows that having these topographic structures does not mean the DSA will be impeded, defect less lamellae structure can still be obtained if given proper conditions [14]. This property can bring out the question that how the substrate topography will affect the performance of BCP DSA on the top of it instinctively.

For lamellae, critical dimension is the PS width printed on resist, line space variation is the difference between PS and PMMA, both measured at a specific height from the substrate. After the lamellae established on the substrate, the PMMA domains will be etched off using dry-etching method. The remaining PS domains will then be used in the following manufacture process. As a result, to get a line-space pattern that can be used in producing materials with better integrated circuit performance to apply in micro electronic devices, the critical dimension (CD) of each PS domain, as well as the space distance between PS domains should not be different a lot[15,16]. In another word, the CD variation and line space variation should be minute enough to ensure the quality of later products. Our previous research has focused on this etching process [17]. It can change the height and roughness of remaining PS

domains, but it can barely change CD and space distance. CD variation for PS domain and line space variation are issues that needed to be concerned since PS domains have different physical and chemical environments with PMMA and between themselves, based on whether the domain is on the top of PS-attractive area (pinned area) or on the top of neutral area (unpinned area). Because high line edge roughness (LER) means the edges will hinder the electrons transfer in the tunnel more severely, as a result, jeopardize the electronic devices performance[18]. LER is always a property that people are trying to decrease to achieve wider BCP DSA commercialization. The roughness values were calculated using 3σ method, which means it is 3 times the beads standard deviation from center edge line[19].

Some relative researches have done in order to eliminate CD variation in the manufacturing process[20,21], others investigated substrate's topography effect on the period pattern formation[22-24]. Tamar Segal-Peretz et al combined scanning transmission electron microscopy (STEM) and coarse grain simulations to get the 3D structure on a topographical templates and studied the influence of template topography on defectiveness formation[25]. Julia Cushen et al studied BCP DSA on a new double patterned sidewall scheme, it applied a different topography to lower the resolution demands on the guideline lithography. But they mainly focused on lamellae roughness and defectiveness on this new template[26]. Rarely researches were focused on the templates' properties effect on the CD variation and line space variation. This research will fill that gap, the influence of template topography and its interaction strength with BCP on CD and line space variation will be investigated. Roughness is also calculated and compared on different substrate topography. On top of that, the

influence of PS/PMMA ratio in BCP were investigated. Since the PS pattern scale is under 20nm, it would be nearly impossible to create the different substrates with a minor topographical variation precisely in experiment, quantitatively control the interaction strength via changing etching condition is also tough. Therefore, CGMD simulation method is applied. The course grained size can be adjusted to a value that is able to represent the tiny difference on substrate and resulted BCP DSA morphology, but not too computational expensive at the same time.

3.2 Methodology

A topographic substrate was applied for LiNe flow process as shown in figure 3.1. Yellow part (pinned area) is cross-linked PS, this area is attractive to PS while repulsive to PMMA and its width A (pinned width) was simulated to be 15nm ($0.53L_0$), 18nm ($0.64L_0$) and 20nm ($0.71L_0$). The blue part (unpinned area) is random distributed hydroxy terminated PS and PMMA short brushes in which the amount of PS and PMMA beads are kept the same, it is neutral to BCP. The grey part (inclined wall) is also cross-linked PS, however, after break through etching in LiNe flow, this part gets polarized, so it is more attractive to PMMA. Considering that in the spin coating process to add brush onto the substrate, some brush will cover the inclined wall, here it is assumed to be neutral as well. It can also be changed to other attractive capability to simulate a 3-tune system. Width B (inclined wall distance) was simulated to be 30nm and 35nm. The raised height of pinned area over unpinned area (gap) was

simulated to be 3nm or 4nm. The periodic length of substrate was set to be 90nm to stay the same with experimental condition.

Those 3*2*2 topography parameters were all combined with each other in the simulation. For the systems perform the best, more topography parameters were carried out, for example, pinned width A equals to 22nm and gap C equals to 2nm or 5nm. The optimized topography systems are also be used to study the effect of interaction strength and PS/PMMA ratio in BCP. Density multiplication is 3, which means in every substrate patterning, there are 3 domains each for PS and PMMA. 28nm above the blue neutral substrate, there is a single flat neutral layer (top wall), it forms a 90nm * 90nm * 28nm simulation box together with the substrate to prevent BCP beads from moving away, this neutral layer and BCP are both not shown in figure3.1. The boundary on X and Y directions are periodic boundaries.

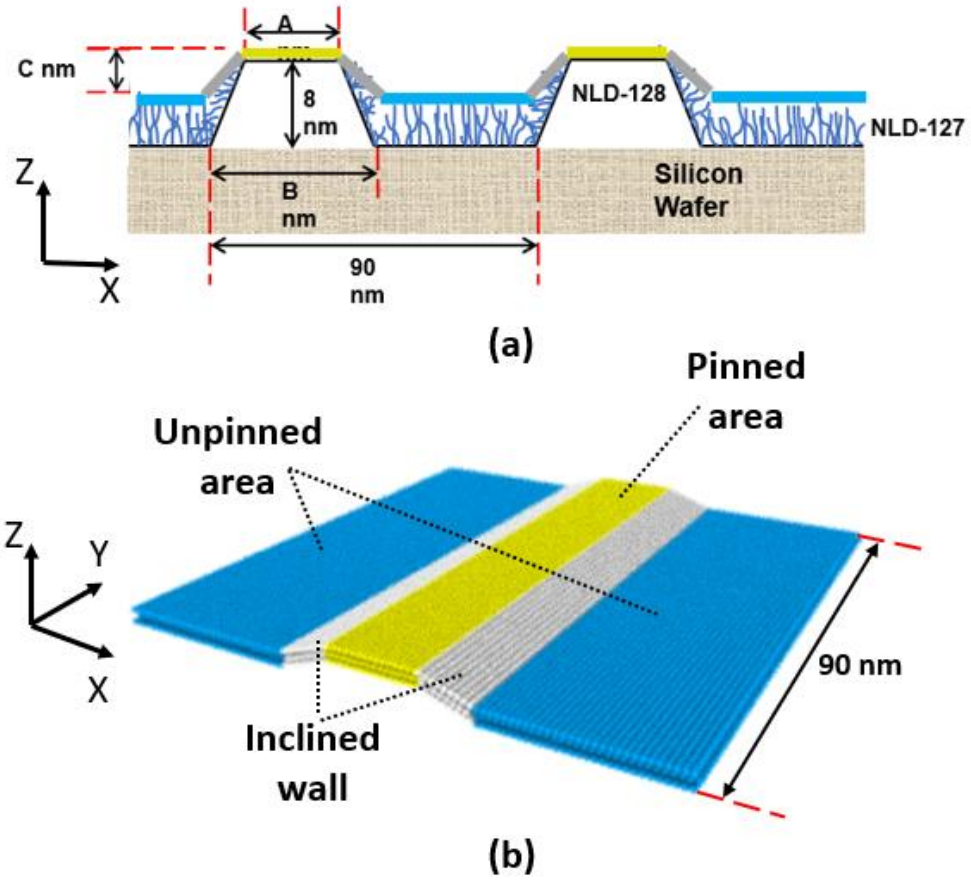

Figure3.1. a) Illustration of substrate parameters; b) CGMD substrate with topography

Different substrate systems were named using their topographic parameters in an order of CAB as in figure3.1. For instance, if the pinned width is 15nm, the inclined wall distance is 30nm and the gap is 3nm, then this system will be named 31530 system.

The polymer chain is modeled as AB block with both monomer radii σ' equals to 0.5nm. Block A has 4 PS monomers in one bead while block B contains 4.5 PMMA monomers in one bead. This difference in course graining is to represent the difference in bulk density for those two monomers. At the beginning when studying the

topography influence, on average, each polymer chain contains 63 PS beads (~26,000 g/mol) and 58 PMMA beads (~26,000 g/mol), the chain length is corresponding to a Poisson distribution with a PDI = 1.01 as shown in figure3.2. Later when investigating the beads ratio in BCP, the PDI is kept 1.0, which means the BCP only contains one molecular weight and one PS/PMMA ratio in each trial. And the following PS/PMMA molecular weight ratio trials were studied: 50/50 (PS~26,000 g/mol, PMMA~26,000 g/mol), 49/51 (PS~25,400 g/mol, PMMA~26,600 g/mol), 48/52 (PS~24,600 g/mol, PMMA~26,600 g/mol), 45/55 (PS~22,900 g/mol, PMMA~27,900 g/mol) and 43/57 (PS~21,600 g/mol, PMMA~28,800 g/mol). The beads number density was always kept the same at ~0.85 beads/nm^3, in different topography systems, due to the difference in available space, the total beads number were changed accordingly. BCP with those molecular weights corresponding to a L_0^{exp} ~ 28nm. The glass transition temperature represented in LJ units is 0.3.

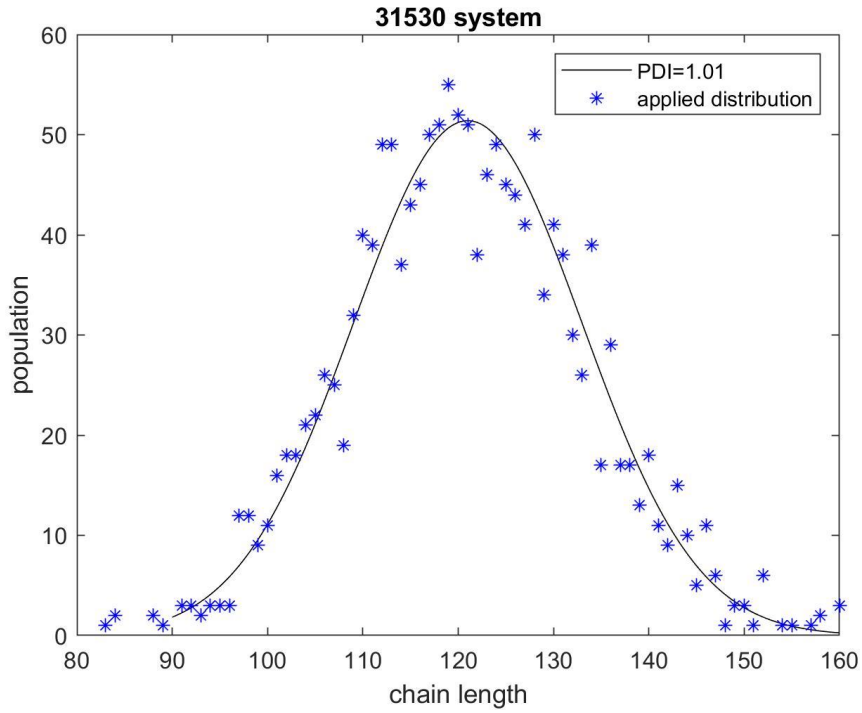

Figure3.2. PS-b-PMMA polymer chain length distribution in a X*Y*Z=90nm *90nm *28nm 31530 system. Other systems have the same polymer molecular weight distribution unless mentioned to be single molecular weight BCP.

FENE bond was applied between adjacent BCP beads in a same chain as the short-range interaction, their interaction potential follows equation 3.1. K = 30 εσ'-2 is the spring constant for the bond and Rmax = 1.5σ' is the maximum bond extensibility[27].

$$U_{FENE}(r) = -0.5KR_{max}^2 \ln\left[1 - (\frac{r}{R_{max}})^2\right] \qquad \text{(eqn.3.1)}$$

The thermostat applied is Nose-Hoover. The attractive long-range interaction is governed by a tail- corrected Lenard Jones interaction as equation 3.2 while the repulsive long-range interaction is in accordance to Weeks-Chandler-Anderson (WCA) potential as equation 3.3.

$$U_{attractive}(r) = 4\varepsilon[\left(\frac{\sigma\prime}{r}\right)^{12} - \left(\frac{\sigma\prime}{r}\right)^{6} + S_{LJ}(r)] \qquad r < 2.5\sigma\text{'} \quad \text{(eqn. 3.2)}$$

$$S_{LJ}(r) = \begin{cases} C, & r < 1.9149\sigma' \\ \frac{a}{3}(r - r_1)^3 + \frac{b}{4}(r - r_1)^4 + C, & 1.9149\sigma' < r < 2.5\sigma' \end{cases}$$

$$U_{repulsive}(r) = 4\varepsilon[\left(\frac{\sigma\prime}{r}\right)^{12} - (\frac{\sigma\prime}{r})^{6}] \qquad r < 2^{1/6}\sigma\text{'} \quad \text{(eqn. 3.3)}$$

Those interactions are the same as what previous study applied and have been verified[17,28]. Default Lenard Jones interaction parameters are listed in table 3.1. Any interaction with the distance larger than maximum cut-off distance = 2.5σ' will not be calculated, as a result, the substrate thickness was chosen to be 3σ'. The long-range potential will not be calculated if 2 beads are in the same chain and there are more or equal to 3 beads between them.

Between beads	Amplitude	Type	Representation
PS, PS	0.15	attractive	$\varepsilon_{PS\text{-}PS}$
PS, PMMA	0.15	repulsive	$\varepsilon_{PS\text{-}PMMA}$
PMMA, PMMA	0.15	attractive	$\varepsilon_{PMMA\text{-}PMMA}$
PS, pinned area	0.15	attractive	$\varepsilon_{PS\text{-}pinned}$
PMMA, pinned area	0.15	repulsive	$\varepsilon_{PMMA\text{-}pinned}$
BCP, unpinned area	0.15	attractive	$\varepsilon_{BCP\text{-}unpinned}$
BCP, top layer	0.15	attractive	$\varepsilon_{BCP\text{-}top}$

Table 3.1. Default LJ parameters used in simulation. Type "attractive" used equation 3.2 to calculate long range potential while "repulsive" used equation 3.3.

At the beginning of each trial, the BCPs were totally random distributed in the simulation box. After annealing at T_{anneal} = 1.2 with the parameters and interactions above for few million steps with a timestep τ = 0.01, the defect free lamellar patterns

can be achieved. Then the system was cooling to T_{cool} = 0.15 to obtain a low fluctuation lamellae structure. As shown in figure 3.3c, this after cooling structure is lower on roughness and can be converted to product if given further treatments like etching. The anneal temperature is just below the critical temperature in order to decrease the required annealing time while maintaining the capability of tracking the beads to prevent they from getting lost in one timestep due to extreme high kinetic energy. The cooling temperature is below the glass transition temperature. Both temperatures are in the similar range as experimental temperature thus are both able to represent the experimental process.

After the system is equilibrated below T_g, the PS domain width on top of pinned area (pinned domain width), the PS domain width on top of unpinned area (unpinned domain width) and PMMA domain width (space width) were calculated using edge detection method[13]. LER of pinned and unpinned domains were also investigated. Note that all those widths and roughness are averaged through Z axis. The unpinned domain width is averaged among two unpinned PS domains in a period. The space width is averaged among two PMMA domains that are not on the edge of simulation box to eliminate the effect of periodic boundaries. The annealing and cooling processes for 41835 system are shown in figure 3.3 as a demo.

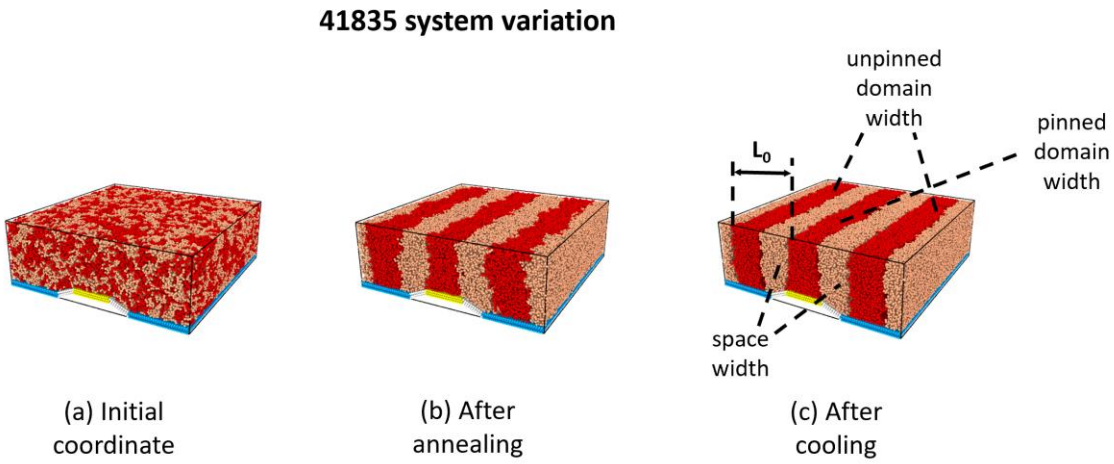

Figure3.3. 41835 system through the whole BCP DSA process and an illustration for meaning of different widths. a) System initial coordinate; b) System after annealing; c) System after cooling.

3.3 Results and discussion

Pinned domain width, unpinned domain width, space width and roughness data for pinned and unpinned width were calculated and shown in figure 3.4. The widths are defined as the distance from the surface of one edge bead to the surface of the other edge bead, not the distance between the center of beads. The reason space domain's LER was not calculated is because space domain has the same edge as PS domain, there is no need to repeat calculation.

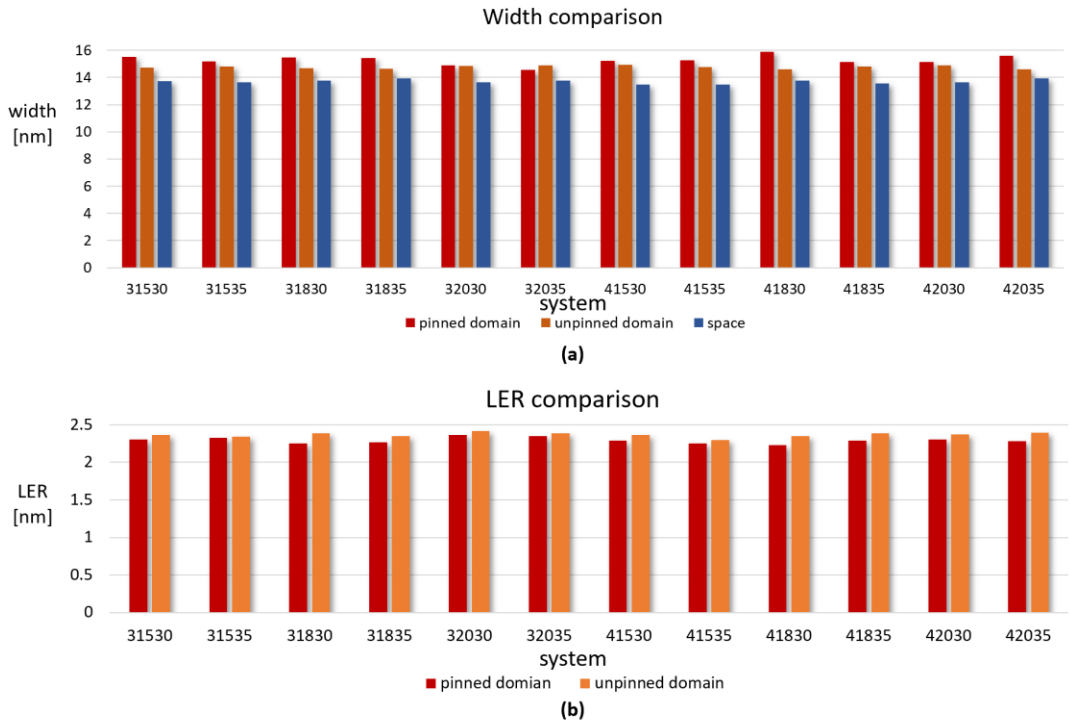

Figure3.4. Bar graph for different domains widths and roughness on topographic substrate. a). width in different systems, b). LER in different systems.

From figure 3.4a, in different topographic systems, the space width is always 1.5~2 nm shorter than that in pinned and unpinned domain (line space). This issue can be solved by varying PS/PMMA ratio, which will be discussed later. The CD variation is hard to distinguish from this bar graph, further analysis is given in figure3.5. From figure 3.4b, the variations between LER in pinned and unpinned domains were all tiny but unified. A conclusion can be made that topographic structure does not have a large effect on roughness while pinned domain always has relatively smoother edges than the unpinned domain. The explanation is on the top of directed area (where pinned domain lies), the directed force reaches its maximum value thus could form a smoother edge domain.

Figure 3.5 shows the critical dimension varied with gap, pinned width and inclined wall distance. Critical dimension equals to pinned domain width minus unpinned

domain width. Although the CD variations were not different on a large scale, it is still worth finding the better topography to lower it as much as possible considering the lamellae scale is under 20nm. From figure 3.5a, the gap influence on CD variation still requires further studying since the results are not consolidating. Figure 3.5b shows that as pinned width deviates from PS periodic length (~15nm), the corresponding CD variation increases at first and then decreases more, this CD decrease is related with tapering effect, it does not imply a larger pinned width is preferred. Figure 3.5c implies that a 35nm inclined wall distance performs better than a 30nm one.

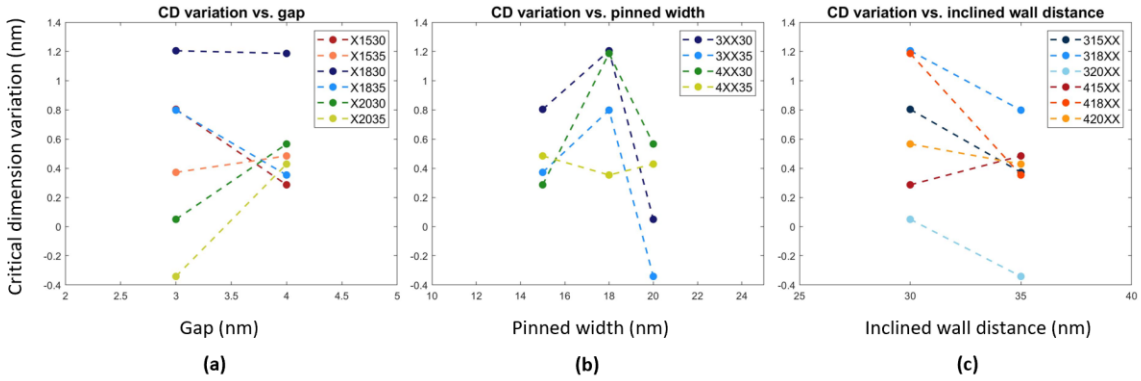

Figure3.5. CD variation with different a) gap, b) pinned width, c) inclined wall distance.

Obviously, in figure 3.5, data for system with a 20nm pinned width performs weird. For example, in figure 3.5a, for 20nm system, CD variation increases as gap getting larger and 32035 system has a negative CD. These unusual performances related with tapering effect. For pinned domain, although the average widths are similar through the systems, as pinned width getting larger, the width at the bottom increases accordingly. This tapering effect can be observed clearly in the width vs. different

height from the substrate graph (figure 3.6). In a system with a large pinned width, as the layer height from bottom gets higher, the domain width shrinks. In the followed etching process, the whole PMMA parts as well as the top PS parts will be etched off, as a result, the averaged pinned domain widths will become higher after etching in those systems. The unpinned domain widths are uniform through z axis, it will not change much. Therefore, the CD variation will become larger for those systems after etching. Also, a z-axis ununiform domain cannot lead to an industrial preferred line space pattern. As a result, in figure 3.5b, although pinned width 20 system seems better in CD variation, pinned width 15 system is more promising.

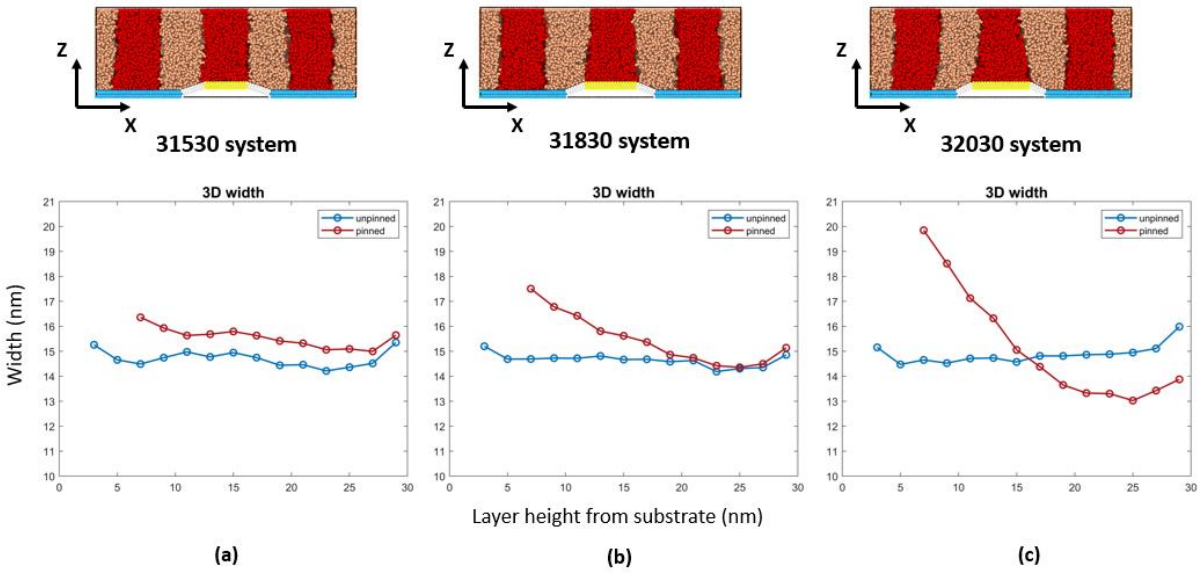

Figure 3.6. PS domain viewed from x-z direction and their widths on different height from substrate for a) 31530 system, b) 31830 system, c) 32030 system. Blue line is unpinned domain width, red line is pinned domain width.

In the three substrate topographic parameters, gap is the one relative easier to change compared with inclined wall distance. But the gap influence on CD variation is vague if solely based on 2 value trials. Therefore, more research towards gap were required, 2 more systems (21535, 51535) with optimized pinned width (15nm) and inclined wall distance (35nm) were carried out. The results are shown in figure 3.7. There is not a linear relation, instead, an optimized gap range (3nm ~ 4nm) exists.

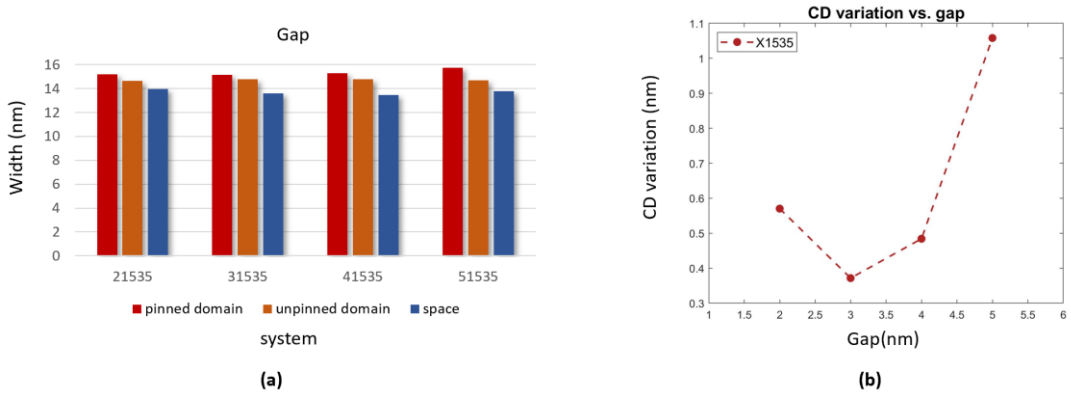

Figure 3.7. Gap influence on CD variation in X1535 systems. a) widths for different domains, b) CD variation vs. gap.

Integrated all the factors together, 31535 and 41535 are among the best 2 topography systems. These 2 systems were used in the following research. The 31535 system was chosen to be the one to investigate the influence of interaction strength on CD variation. Interaction parameter between pinned area and BCP was set to vary from 0.1 to 1.0 while other parameters were kept at 0.15. Those are all LJ units, since in industry, those parameters will not be measured and controlled directly, there is no problem here just using LJ units for the convenient of simulation. Interaction strength has a linear negative effect on CD variation as illustrated in figure 3.8, therefore in

order to get a low CD variation pattern, the cross-linked PS composition and break through etching conditions ought to be altered to get a small interaction strength with BCP. It can be explained that too strong a pinned area will tend to attract more PS towards it, and lead to a larger CD variation. So as long as the guiding force is large enough to help BCP form lamellar structure in the right direction, a weaker force is better for the lamellae quality. And interaction strength does not appear obvious influence on roughness values. Later in the simulation, the interaction strength was still set to be 0.15 instead of the best performance 0.1 to prevent repeating the same topographic trials.

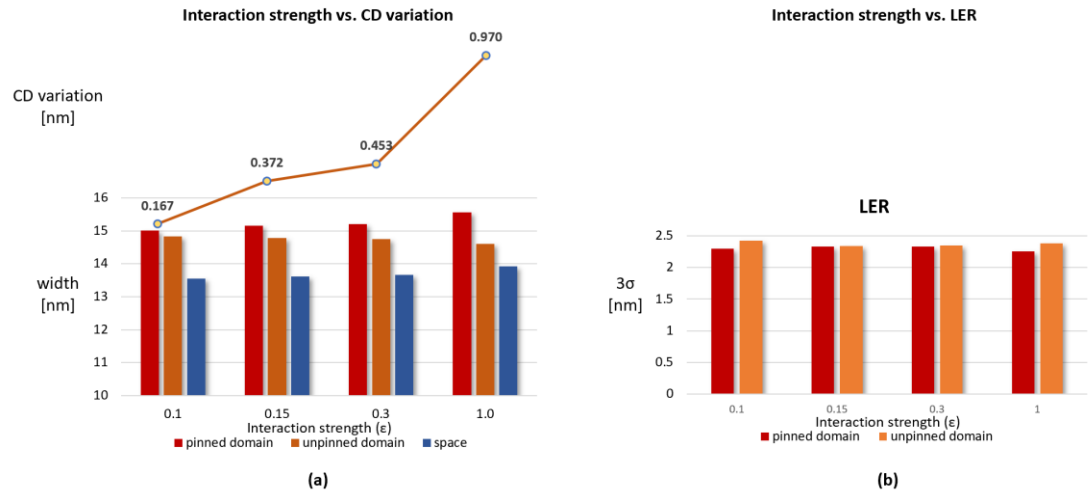

Figure 3.8. 31535 system under the influence of different interaction strength, ε. a) each domain width and CD variation; b) LER values.

The 41535 system was used for the following BCP ratio influence simulations, which mainly aimed at decreasing the line space variation. The results are shown in figure 3.9. Note that the BCPs used here are mono molecular weight, their total molecular weights are all around 50,000 g/mol, the detailed information can be found

in the methodology section of this chapter. The interaction strengths here are all 0.15 to keep harmony with topographic trials. Among the ratio we studied, PS/PMMA equals to 48/52 molecular weight ratio leads to the smallest line space variation. The corresponding PS molecular weight is approximately 24,600 g/mol while PMMA is 26,600 g/mol. The PS/PMMA ratio does not have an obvious influence on roughness.

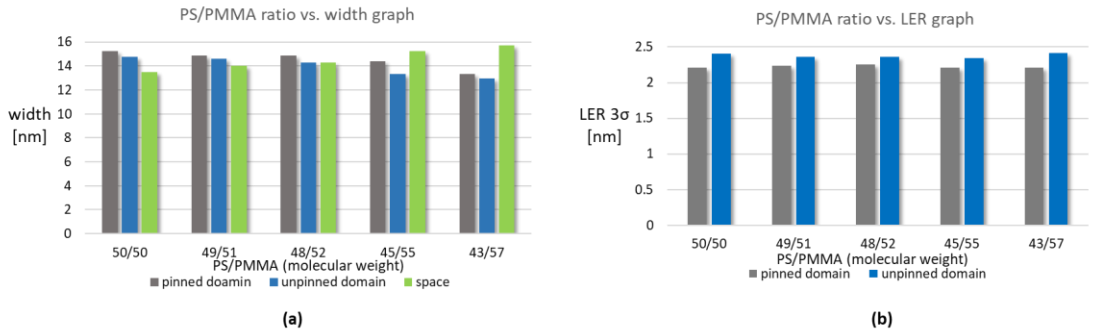

Figure 3.9. When changing the PS/PMMA molecular weight ratio in BCP in a 41535 system, a) different domain width, b) different domain LER value.

In the optimized 48/52 ratio BCP trials, some topography effect, especially pinned area width effect, have been investigated. To find a way solving the tapering effect mentioned previously, some trials that have the pinned area edge beads covered have been studied. This is to simulate the scenario that some neutral brushes at the inclined wall or bottom level of the substrate are covering the edge of pinned area. In another word, decreasing the pinned area while keeping the same topography structure. Those following trials were carried out: 4 nm at the edge of a 42235 system's pinned area was covered, 8nm at 42235 system, 10 nm at 42235 system and 3 nm at 41535 system. Results are shown in figure 3.10.

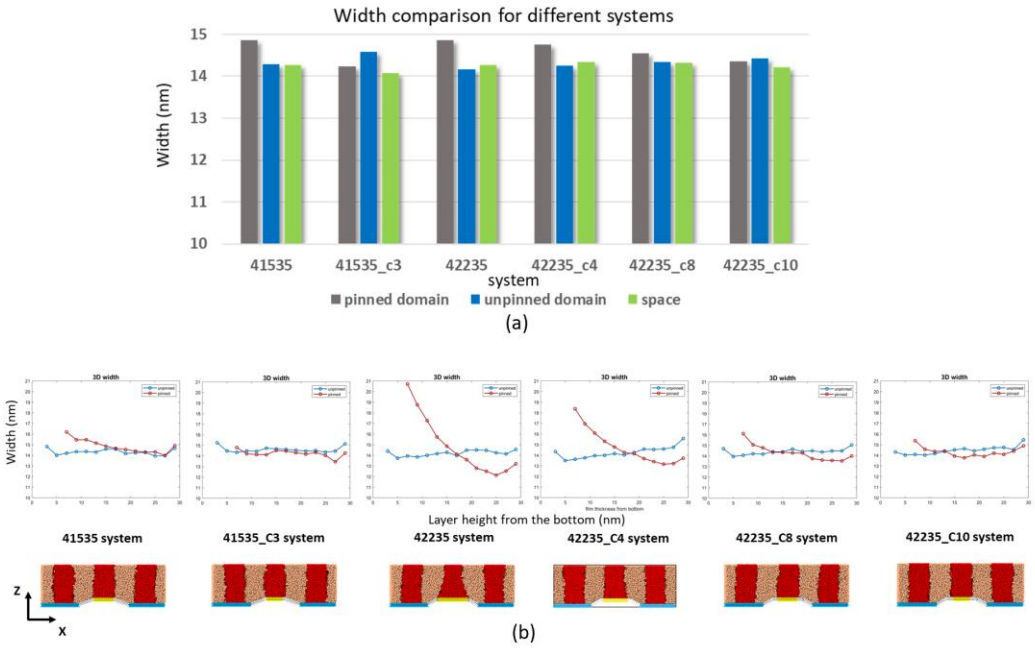

Figure 3.10. Width in 41535, 42235 and their covering systems. a) bar graph for width comparison; b) PS domain viewed from x-z direction and their widths on different height from substrate. Blue line is unpinned domain width, red line is pinned domain width.

Due to the abnormal expansion of the bottom part of pinned domain and the extreme tapering effect, 42235 system has similar CD variation with 41535 system. Compare the covered system with original systems, covered system could eliminate tapering effect dramatically and balance the width between domains on the top of pinned area and unpinned areas, thus decrease the CD variation. Actually, the 42235 system with 8nm and 10nm pinned area being covered by a PS/PMMA mass ratio equals to 0.925 BCP both are the best systems among all what we have studied. In the covered system, the direct decrease of the pinned domain bottom part width is always smaller than the covering width, for example, in the cover 3nm system (the second

column in figure 3.10b), the bottom layer width went down for around 1.5nm; in cover 8nm system (the fifth column in figure 3.10b), the width went down for 5nm; in cover 10nm system (the sixth column in figure 3.10b), the width went down for 5.5nm. The results imply that comparing with a shorter pinned width system without covering, covering part of the pinned area in a larger pinned width system can reach to a better result in terms of CD variation without tapering effect (41535 and 42235_C8 system). If the available pinned width (pinned width minus covered length) is a little bit smaller than PS L_0 which is around 15nm (41535_C3 and 42235_C10 system), although the CD variation will be a negative value, there is no "anti-tapering" effect happening, and those trials perform better than available pinned width larger than PS L_0 trial (42235_C4 system). Take the etching process into condition, after the top parts are etched off, the CD variation for remaining parts will be closer to 0, lead to a better pattern for the following manufacture process. Further research on different covered system is still needed, for example, according to figure 3.5b, there is chance that pinned width equals to 20nm systems will perform better if the tapering effect is eliminated. It is still required many efforts to find the optimized available pinned width in combination with other parameters like substrate topography and interaction strength for the best CD variation performance.

4. Conclusion

With the aim of decreasing the CD variation and line space variation, to get a evenly distributed line space pattern for application in semiconductor, the effect of

topographic substrate, different monomer ratio and interacting strength on CD variation and roughness have been investigated via a large scale CGMD simulation method. The substrate topography accuracy can be controlled in 1 nm, which is a lot more accurate than that in the experiment. The precise control on hard-to-control parameters and 3D structure detection and analyzing method through out the whole DSA process are the 2 main advantages of this simulation. PS-b-PMMA copolymer starts from totally random distribution, after annealing, it forms lamellae structure, and after cooling below glass transition temperature, it forms smooth lamellae structure that can be used for etching. By calculating different domains widths and LER through the whole domain, the performance of each trial under different conditions (topographic structure, monomer ratio, interacting strength) can be compared.

Topographic substrate has some effect on LER, but that effect is too minute to focus (order of 0.1 nm) at current BCP DSA accuracy. Pinned domain always has a lower LER than unpinned domain due to the inherent property of DSA. Some methods other than changing substrate topography are needed to decrease LER and obtain a smoother lamellae structure that is preferred in application.

There is an optimized height difference (called gap in this paper) between neutral substrate and pinned area existing in minimizing the CD variation, this optimized gap distance is around 3 to 4 nm. Increasing pinned width from PS L_0 will cause tapering effect, although the average CD variation seems smaller in a larger pinned width system, it should be kept at a value close to PS L_0. This effect can explain the unusual behavior of pinned width equals to 20nm systems. In the range we investigated, the

inclined wall distance has a positive effect on decreasing CD variation, increasing it from 30nm to 35nm can lead to a better lamellae structure from CD perspective.

Changing the PS/PMMA ratio is a promising way in decreasing line space variation, the best mass ratio we found is around PS/PMMA ~ 0.925/1 (24,600 $g.mol^{-1}$/26,600 $g.mol^{-1}$). Lowering the interaction strength between pinned area and BCP is another good way to decrease CD variation, the restrict factor for lowering interaction strength is the guiding force must be strong enough to guide a successful BCP DSA. But those methods do not have much effect on roughness neither.

Covering the edge of pinned area is a good way to eliminate tapering effect as well as CD variation, it gave the best performance trials in our research. The optimized available pinned width should be lower than PS L_0 in a small scale. Therefore, if the substrate brushes are long or the gap is small, although it is relatively difficult to control the covering, it would be a promising direction to make pinned area larger than PS periodic length. More researches on different covered and uncovered substrates are still worth carrying out in the future. Replacing the steady substrate beads with flexible brush short chains is a promising method to better simulate the BCP DSA process. Relate the investigated parameters in this research with real experimental parameters is also crucial in guiding the BCP DSA experiment. This is out of the scope of this chapter, but the direction of changing those factors has been pointed out.

REFERENCES

(1). Jeong SJ, Kim JY, Kim BH, Moon HS, Kim SO. Directed self-assembly of block copolymers for next generation nanolithography. Materials Today. 2013 Dec 31;16(12):468-76.

(2). Liu CC, Ramírez-Hernández A, Han E, Craig GS, Tada Y, Yoshida H, Kang H, Ji S, Gopalan P, de Pablo JJ, Nealey PF. Chemical patterns for directed self-assembly of lamellae-forming block copolymers with density multiplication of features. Macromolecules. 2013 Feb 11;46(4):1415-24.

(3). Mack CA. Field guide to optical lithography. Bellingham, Washington, USA: SPIE Press; 2006 Jan 24.

(4). Wu B, Kumar A. Extreme ultraviolet lithography: a review. Journal of Vacuum Science & Technology B. 2007 Nov 1;25(6):1743-61.

(5). Ruiz R, Kang H, Detcheverry FA, Dobisz E, Kercher DS, Albrecht TR, de Pablo JJ, Nealey PF. Density multiplication and improved lithography by directed block copolymer assembly. Science. 2008 Aug 15;321(5891):936-9.

(6). Cheng JY, Rettner CT, Sanders DP, Kim HC, Hinsberg WD. Dense self-assembly on sparse chemical patterns: Rectifying and multiplying lithographic patterns using block copolymers. Advanced Materials. 2008 Aug 18;20(16):3155-8.

(7). Kim SO, Solak HH, Stoykovich MP, Ferrier NJ, de Pablo JJ, Nealey PF. Epitaxial self-assembly of block copolymers on lithographically defined nanopatterned substrates. Nature. 2003 Jul 24;424(6947):411-4.

(8). Liu CC, Han E, Onses MS, Thode CJ, Ji S, Gopalan P, Nealey PF. Fabrication of lithographically defined chemically patterned polymer brushes and mats. Macromolecules. 2011 Mar 18;44(7):1876-85.

(9). Liu CC, Ramírez-Hernández A, Han E, Craig GS, Tada Y, Yoshida H, Kang H, Ji S, Gopalan P, de Pablo JJ, Nealey PF. Chemical patterns for directed self-assembly of lamellae-forming block copolymers with density multiplication of features. Macromolecules. 2013 Feb 11;46(4):1415-24.

(10). Gronheid R, Doise J, Bekaert J, Chan BT, Karageorgos I, Ryckaert J, Vandenberghe G, Cao Y, Lin G, Somervell M, Fenger G, Fuchimoto D. Implementation of templated DSA for via layer patterning at the 7nm node. Proc. SPIE. 2015, 9423: 942305.

(11). Liu CC, Franke E, Lie FL, Sieg S, Tsai H, Lai K, Truong H, Farrell R, Somervell M, Sanders D, Felix N, Guillorn M, Burns S, Hetzer D, Ko A, Arnold J, Colburn M. DSA patterning options for FinFET formation at 7nm node. Proc. SPIE. 2016, 9777: 97770R.

(12). Liu G, Delcambre SP, Stuen KO, Craig GSW, De Pablo JJ, Nealey PF, Nygard K, Satapathy DK, Bunk O, Solak HH. Mechanism and dynamics of block copolymer directed assembly with density multiplication on chemically patterned surfaces. Journal of Vacuum Science & Technology B. 2010, 28(6), C6B13-C6B19.

(13). Park S, Lee DH, Russell TP. Self-assembly of block copolymers on flexible substrates. Advanced Materials. 2010, 22: 1882-1884.

(14). Williamson LD, Seidel RN, Chen X, Suh HS, Delgadillo PR, Gronheid R, Nealey PF. Three-tone chemical patterns for block copolymer directed self-assembly. Applied Materials & Interfaces. 2016 Jan 8;(8):2704-2712.
(15). Yin Y, Lu Y, Gates B, Xia Y. Template-assisted self-assembly: a practical route to complex aggregates of monodispersed colloids with well-defined sizes, shapes and structures. Journal of American Chemical Society. 2001, 123(36): 8718-8729.
(16). Kraus T, Malaquin L, Schmid H, Riess W, Spencer ND, Wolf H. Nanoparticle printing with single-particle resolution. Nature Nanotechnology. 2007, 2: 570-576.
(17). Pinge S, Qiu Y, Monreal V, Baskaran D, Ravirajan A, Joo YL. Three-dimensional line edge roughness in pre- and post- dry etch line and space patterns of block copolymer lithography. Physical Chemistry Chemical Physics, 2020, 22: 478-488.
(18). Leung G, Lai L, Gupta P, Chui CO. Device-and circuit-level variability caused by line edge roughness for sub-32-nm FinFET technologies. IEEE Transactions on Electron Devices. 2012 Aug;59(8):2057-63.
(19). Bosse AW, Lin EK, Jones RL, Karim A. Interfacial fluctuations in an ideal block copolymer resist. Soft Matter. 2009;5(21):4266-71.
(20). Asbahi M, Wang FK, Dong Z, Yang JKW, Chong KSL. Directed self-assembly of sub-10nm particle clusters using topographical templates. Nanotechnology. 2016, 27(42): 424001.
(21). Schmid G, Farrell R, Xu J, Park C, Preil M, Chakrapani V, Mohanty N, Ko A, Cicoria M, Hetzer D, Somervell M, Rathsack B. Fabrication of 28nm pitch Si fins with DSA lithography. SPIE Press; 2013 Mar 26.
(22). Cheng JY, Ross CA, Thomas EL, Smith HI, Vancso GJ. Templated self-assembly of block copolymers: effect of substrate topography. Advanced Materials. 2003, 15(19): 1599-1602.
(23). Yi H, Bao XY, Zhang J, Bencher C, Chang LW, Chen X, Tiberio R, Conway J, Dai H, Chen Y, Mitra S, Wong HSP. Flexible control of block copolymer directed self-assembly using small, topographical templates: potential lithography solution for integrated circuit contact hole patterning. Advanced Materials. 2012, 24: 3107-3114.
(24). Yi H, Latypov A, Wong HSP. Computational simulation of block copolymer directed self-assembly in small topographical guiding templates. San Jose, California, USA: SPIE Press; 2013 Mar 26.
(25). Segal-Peretz T, Ren J, Xiong S, Khaira G, Bowen A, Ocola LE, Divan R, Doxastakis M, Ferrier NJ, Pablo J, Nealey PF. Quantitative three-dimensional characterization of block copolymer directed self-assembly on combined chemical and topographical prepatterned templates. ACS Nano. 2017, 11: 1307-1319.
(26). Cushen J, Wan L, Blachut G, Maher MJ, Albrecht TR, Ellison CJ, Willson CG, Ruiz R. Double-patterned sidewall directed self-assembly and pattern transfer of sub-10 nm PTMSS-b-PMOST. ACS Applied Materials and Interfaces. 2015, 7: 13476-13483.

(27). Kremer K, Grest GS. Dynamics of entangled linear polymer melts: A molecular-dynamics simulation. The Journal of Chemical Physics. 1990 Apr 15;92(8):5057-86.
(28). Towns J, Cockerill T, Dahan M, Foster I, Gaither K, Grimshaw A, Hazlewood V, Lathrop S, Lifka D, Peterson GD, Roskies R. XSEDE: accelerating scientific discovery. Computing in Science & Engineering. 2014 Sep 1;16(5):62-74.

Chapter 4. FUTURE WORK AND CHALLENGES

4.1 Challenges in BCP DSA Simulation

To keep the previous description smooth and away from redundant, some details and challenges that will appear in the process of BCP DSA simulation are neglected. Those details and challenges will be mentioned here.

4.1.1 Warm up steps

Based on different system topographies or BCP properties, different BCP initial coordinates were generated using MATLAB. This process has nothing to do with thermodynamics, as a result, there would be some overlapping between beads. If normal simulation interaction potential, Lennard Jones potential, was applied directly, the simulation would be jeopardized due to the extremely high interaction force generated by overlapping. Therefore, a process called "warm up" was applied between initial coordinates and annealing simulation. In this process, a different interaction potential energy equation, "soft", was used. As equation 4.1 illustrates, this soft potential is a cosine equation, it does not blow up when distance r goes to 0. E is potential energy, r_c is cut off radius and A is a pre-factor that can be varied with time in order to make this potential very soft at the beginning and get harden over time.

$$E = A\left[1 + cos\left(\frac{\pi r}{r_c}\right)\right] \qquad \text{(equation 4.1)}$$

In our simulation, pre-factor A was set to be varied between 10 and 200 with time, and the cut off radius r_c is 2.5σ. Since the aim of warm up process is to avoid

overlapping, there is no required total steps as long as the followed annealing process can be carried out correctly. But different warm up steps do lead to different beads coordinates at the beginning of annealing steps, and this difference has been shown to have influence on structure. Based on the experience, 1.5 million to 2 million warm up steps were used, these amount of steps can separate the beads completely, and too many steps is a waste of computing resources. Figure 4.1 shows different annealing results starting from different warm up steps.

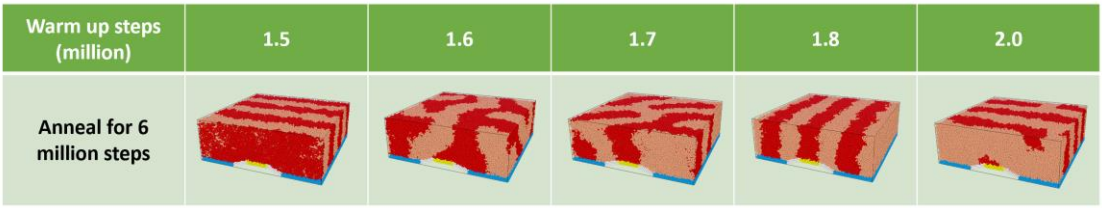

Figure 4.1. A type of mono-distributed BCP that has 51,200 g/mol molecular weight and 48/52 PS/PMMA ratio in each chain, annealing for 6 million steps starting from different warm up steps in a 41535 system.

This “warm up step” is a pure simulation concept, in experiments, there is no need to worry about particles overlapping. Not each warm up step could lead to a defect-free lamellar structure after annealing, that is because the amount of annealing step is finite, the initial coordinate at the beginning of annealing can affect the formed structure. Thermodynamically, the lamellar structure will form (although there might be some defectiveness) if given plenty of time because that structure is the lowest in regard of energy, and that is true in industry. However, in simulation, the time scale is around few nano seconds, and the limitation of computing resources prevents us from

having the luxury of simulating at the experimental time scale, which is of few minutes. Because there is no such thing as “higher energy lamellae”, as long as the defect free lamellae can form, it can be used to investigate BCP DSA properties. Through many trials, an empirical rule of thumb is to have 5 different warm up steps for one trial, if all of those are unable to provide defect free lamellae, it is highly possible that the applied condition is not suitable for lamellae formation. Normally, I use 1.5 million, 1.6 million, 1.7 million, 1.8 million and 2 million of warm up steps for each condition. If more than one warm up steps trials give defect free lamellae, their results will be averaged when doing the analysis.

Insufficient warm up steps may cause bonds breaking during annealing steps due to the close distance between beads. Under which circumstances the remediation is to decrease the length of each time step. If the beads are not severely overlapping, this issue can be solved without starting the annealing from the beginning to save computing resources.

4.1.2 Invisible top wall

In experiment, BCP will not expand on z direction, however, in simulation, this is an annoying issue. It is hard to prevent BCP from moving above the simulation box. And as BCP moves beyond the specified maximum z value, the simulation system will assume those beads are lost and error messages will be feedback.

As a result, in every simulation box, an invisible wall was placed at the top of the box as in figure 4.2. This wall served as a cap, it has neutral interaction strength with BCP directed by tail corrected Lennard Jones potential equation, so it would not

influence the BCP annealing structure while keeping BCP from moving out of the simulation box on z direction. There were no such walls at other edges because on x and y direction, the box is periodic, and at the bottom, there was a substrate. Same as the substrate beads, between these top beads, no interactions were applied and their positions were fixed. The thickness of top layer is only 1 σ because the aim of having this layer is solely preventing trespassing, so there is no need for the top layer to be thicker than the cut off radius.

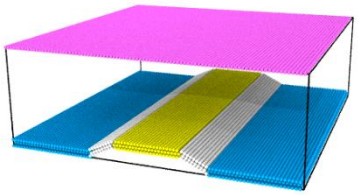

Figure 4.2. The simulation box in a 42035 system. BCP were put between the bottom substrate and the pink top wall.

4.2 Future Work: Flexible BCP Brush Substrate

4.2.1 Background

In real experiment LiNe flow, after break through etching or optional trim etching to form the line space pattern of cross linked PS, the substrate is spin coated using randomly distributed short hydroxy terminated PS-b-PMMA chains. Changing the properties of those short chains (brushes) is the method to control interaction strength

and topography of the substrate. Those properties include but are not limited to brush density, ratio between PS and PMMA in those brushes, brush chain length, which are the properties required more thoroughly investigation in the future work. Other very important aspects people use to change topography lie in etching conditions such as etching time and etch gas composition, etc. But those are beyond the scope of this project.

Previously, the method that was used to investigate those substrate properties is changing the properties directly. For example, the gap distance was set to 2, 3, 4 or 5 nm when generating the substrate. However, in reality, this parameter was controlled via changing the short brush length or density that coated at the bottom of the substrate. The interaction strength between substrate and BCP is also related with substrate details. The ignorance of details can decrease the usage of computing resources while keeping plenty of information that can lead to a defect free lamellae formation, so it is a great way of determining parameters and optimizing the whole BCP DSA process. And now as the optimized system has been found, those details of brushes will be added back to bring the simulation closer to experiment.

On top of that, as mentioned in Chapter 3, it is found that a system which possesses a larger pinned width but with the edge of the pinned area being covered shows a promising direction in lowering the CD variation while avoiding tapering effect. It is easy to simply set the covering widths to be certain values, however, to figure out what brush condition corresponding to those covering widths is not an easy task. It can only be completed with the help of flexible brush substrate system.

4.2.2 Model details

Figure 4.3 shows the substrate before and after putting the spin coated brushes on. The A, B, C are the topographic parameter for silicon wafer and pinned area before brushes were introduced. Note that the parameter B and C have different meaning with those in chapter 3, but A represents the same thing, pinned width. In this initial trial, A was set to be 15nm, B was 30nm, C was 8nm. In figure 4.3b, the red and orange dots on the substrate are the first bead in PS or PMMA brushes.

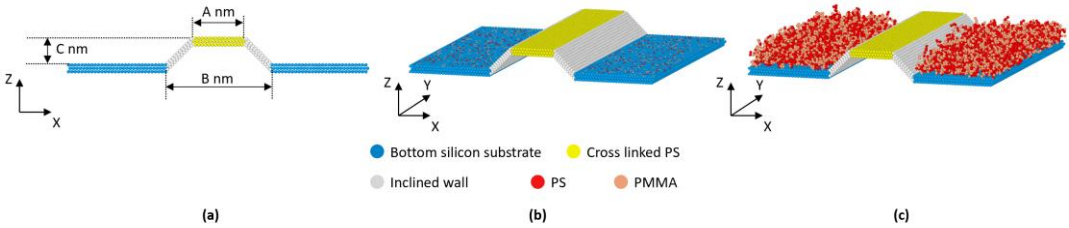

Figure 4.3. Substrate profiles for brush system. (a), front view of the substrate before putting the brush on; (b), perspective view of substrate before putting the brush on; (c), perspective view of substrate after putting the brush on.

Each chain is composed with randomly ordered PS and PMMA beads, and in the shown case, each chain has a length of 16nm, and total brush chain number is 1200. The top layer of the brushes together with the exposed inclined wall and pinned area forms the new substrate for BCP annealing. Chain length and chain density can be changed, in that way, the BCP substrate topography will be modified accordingly. Same as in BCP, the bonds between adjacent beads are FENE bonds, and the

intramolecular potential between same type of beads follows tail corrected LJ potential, energy between different type of beads follows WCA (Weeks Chandler Anderson) potential. The interaction strength ε between those brushes are the same as ε in BCP, which is 0.15 for now. In this brush model, the 6 parameters that require optimize are A, B, C, brush chain length, brush density and interaction strength. This is the future work of this project.

4.3 Challenges in Brush System

When replacing the steady substrate beads with flexible brushes, besides more consumption of computing resources, there are more challenges that needed to or have already been solved.

4.3.1 Too Close Brushes

The first beads of each brush were selective randomly from the bottom substrate, as a result, some adjacent substrate beads might be chosen at the same time, under which condition, the simulation system will be jeopardized for the extreme high potential because the distance is too small. To solve this issue, one more judgement was added into the brush generating code: after one substrate bead is occupied, the 4 beads that attach to it will not be able to be occupied anymore. One substrate example is shown in figure4.4. Note that this is the same trial as in figure4.3 but look from the top. As long as the brush density does not go too high (lower than 2700 brushes on substrate), this method can serve a fair purpose of preventing potential energy explosion.

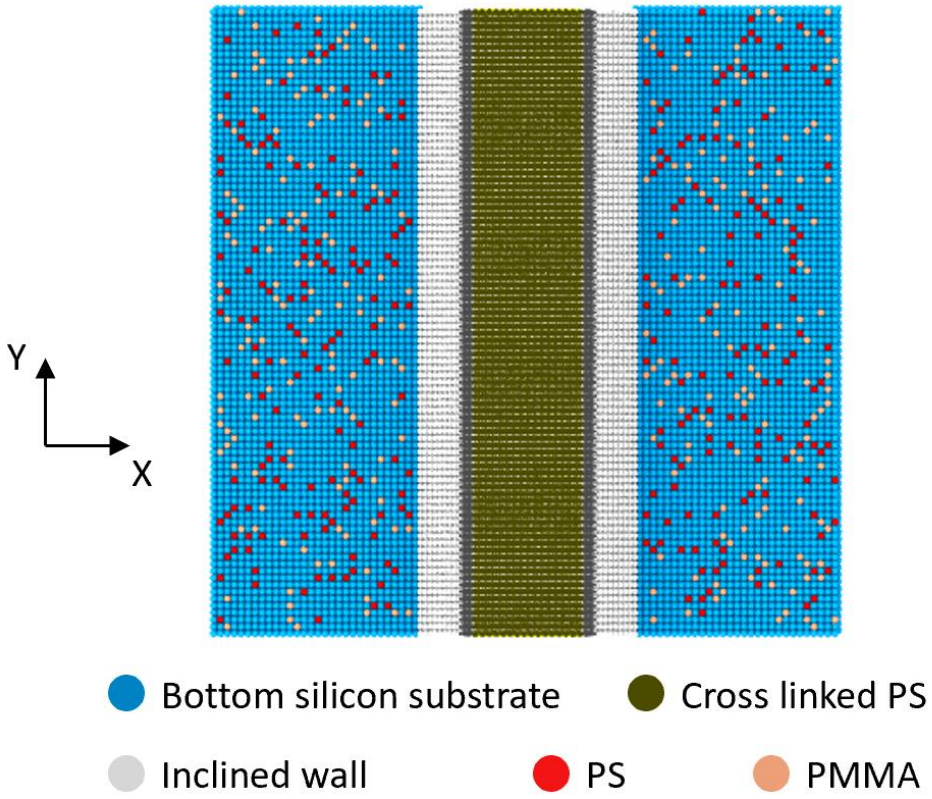

Figure 4.4. Top view of the silicon substrate. The red and orange beads are the beginning bead for each brush chain. The 4 silicon beads adjacent to every occupied bead will not be occupied by other brush chains.

4.3.2 Brush Moving Around During Annealing

In the simulation process, the spin coated brushes at the bottom of silicon substrate will move around during annealing process if not controlled. They may even self assembled themselves or blend into BCP, then the simulation will fail. To prevent the brushes from moving away from the bottom part and blending into BCP, randomly picked silicon substrate beads were replaced with the starting bead of each brush

chain, in which way the brush seem to “grow” from the silicon substrate. Because in the simulation, the substrate beads are fixed, the brushes are restricted in the bottom part of simulation box.

4.3.3 Low Brush Density

In the previous steady substrate trials, the BCP density is kept at around 0.85. This is done by having a top wall and a bottom substrate to form a constraint space. However, for brush chains at the bottom of simulation box, it is not suitable to place a cap to control their morphology because if so, there will not be any differences with the previous steady bead substrate. Without the restriction from a top wall, the bead density in the brush area is very low (< 0.2), in that way, BCP beads which have much higher density at the top will blend into the brushes. Although the simulation will be able to continue under this scenario, chances is very low that a defect free lamellar structure will be able to form. This is an issue that still needs to be solved in the future work of improving the brush substrate model.

4.4 Other Future Plans

4.4.1 Apply Optimized Systems in Experiment

As a few guiding principles in optimizing the template topography, BCP ratio as well as interaction strength have come out, the next crucial step is to apply those guiding rules in experiments and to see the performance of the system. Although the

model validation has been proved before[1], there is no harm checking it again through experiments.

Based on the resources we have, what we are currently doing is having our collaborator EMD Performance Material manufacture the line space pattern samples we request and send to us. Those samples will be characterized and analyzed by us in Cornell mainly using scanning transmission electron microscopy (STEM) with the purpose of obtaining higher resolution images on tiny structures compared with scanning electron microscope (SEM)[2].

On top of that, because the parameters were changed directly in simulation, experiments must be carried out to find the suitable etching conditions corresponding to the different topography and as a result, to complete the last piece of map in using this simulation to guide the BCP DSA process. And with the help of TEM, the accurate details of the substrate can be got, this is also a crucial prerequisite in order to figure out the relation between experimental conditions and simulation parameters.

4.4.2 Simulate Extreme Ultraviolet (EUV) Lithography

It is undeniable that BCP DSA is a promising and energy efficient way of producing minute structure that can be used in the micro electronic devices. It can reach <7nm scale, and although it has issues with roughness and defectiveness, the overall cost and practicality are still relatively low[3-4]. From this perspective, BCP DSA can be a good replacement for currently used deep ultraviolet lithography (DUV) or e-beam lithography method.

However, due to the inherent constraints of BCP DSA, it will be hard to reach even smaller scales. Maybe 7nm is not the limit, but the requirement for next generation integrated circuits will be for sure smaller than what BCP DSA can reach. Inherent constraints also appear in DUV, e-beam and immersion lithography. As the required research input of decreasing the scale of those previous methods is getting tremendous high, EUV lithography becomes the most promising method for next generation micro electronic devices. Like every other fields, there are a huge amount of issues in the EUV field waiting to be solved as mentioned in Chapter 1.

People have done some jobs on the inhomogeneity resist, including its depth-related chemical properties and diffusion rate[5]. Many jobs on simulation have done by using Monte Carlo simulation but the model accuracy is relatively low[6-8]. MD method was also applied in many EUV simulations, it has been proved a practical way of analyzing EUV lithography, although the time scale is smaller than real experiment[9-11]. What we will do in our research is using MD method to simulate this process, especially the resist performance and lithography morphology variation, which can be similar with BCP DSA in many ways. For example, the area under the mask will be etched off like the PMMA domains in BCP lithography; the photons used in EUV lithography will act like Ar/O_2 in the air bombardment process in BCP lithography, one of the main purposes of those two process are both to decrease the LER, etc. In the current phase, some challenges we encounter in the starting of EUV simulation mainly lie in the simulation of photons. Their stochastic properties add some difficulties on the system but the more difficult thing is the “size” of photons in EUV, they perform more like

waves. Those issues will need to be figured out in order to start this future project of EUV lithography.

REFERENCES

(1). Shubham Pinge, et al. Three dimensional line edge roughness in pre- and post-dry etch line and space patterns of block copolymer lithography. Physical Chemistry Chemical Physics, 2020, 22: 478-488.

(2). Tamar Segal-Peretz, et al. Quantitative three-dimensional characterization of block copolymer directed self-assembly on combined chemical and topographical prepatterned templates. ACS Nano, 2017, 11: 1307-1319.

(3). Roel Gronheid, et al. Implementation of templated DSA for via layer patterning at the 7nm node. SPIE Advanced Lithography, 2015, 9423: 942305.

(4). Ioannis Karageorgos, et al. Design strategy for integrating DSA via patterning in sub-7 nm interconnects. SPIE Advanced Lithography, 2016, 9781: 97810N.

(5). Shinichi Nakamura, et al. Photoresist film analysis to investigate LWR generation mechanism. SPIE Advanced Lithography, 2013, 8682: 86821H.

(6). Akinori Saeki, et al. Line edge roughness after development in a positive-tone chemically amplified resist of post-optical lithography investigated by Monte Carlo simulation and a dissolution model. Nanotechnology, 2007, 19: 1.

(7). Gerard M. Schmid, et al. Spatial distribution of reaction products in positive tone chemically amplified resists. Journal of Vacuum Science and Technology B, 2002, 20: 185.

(8). Akinori Saeki, et al. Correlation between proton dynamics and line edge roughness in chemically amplified resist for post-optical lithography. Journal of Vacuum Science and Technology B, 2006, 24: 3066.

(9). Minoru Toriumi, et al. Inhomogeneity of photoacid generators in methacrylate-type EUV resist film studied by molecular dynamics simulation. Japanese Journal of Applied Physics, 2015, 54: 6S1.

(10). Xiaolei Zhang, et al. The effect of soft bake on adhesion property between SU-8 photoresist and Ni substrate by molecular dynamics simulation. Journal of Applied Polymer Science, 2013, 127, (6): 4456-4462.

(11). Katsushi Michishita, et al. Electron beam lithography simulation for sub-10 nm patterning. Japanese Journal of Applied Physics, 2014, 53: 6S.